HHS Public Access

Author manuscript

*Nat Cell Biol*. Author manuscript; available in PMC 2021 May 03.

Published in final edited form as:

*Nat Cell Biol*. 2020 December ; 22(12): 1411–1422. doi:10.1038/s41556-020-00604-7.

# Haematopoietic stem cell-dependent Notch transcription is mediated by p53 through the Histone chaperone Supt16h

**Sophia G. Espanola**[1], **Hyemin Song**[1,2], **Eunjin Ryu**[3], **Aditya Saxena**[4], **Eun-Sun Kim**[2], **Jennifer E. Manegold**[1], **Chanond A. Nasamran**[5], **Debashis Sahoo**[6], **Chang-Kyu Oh**[2], **Cara Bickers**[1], **Unbeom Shin**[3], **Stephanie Grainger**[4], **Yong Hwan Park**[2], **Lauren Pandolfo**[4], **Mi-Sun Kang**[2], **Sukhyun Kang**[2], **Kyungjae Myung**[2,3], **Kimberly L. Cooper**[4], **Deborah Yelon**[4], **David Traver**[1,✉], **Yoonsung Lee**[1,2,3,✉]

[1]Department of Cellular and Molecular Medicine and Section of Cell and Developmental Biology, University of California, San Diego, La Jolla, CA, USA

[2]Center for Genomic Integrity, Institute for Basic Science (IBS), Ulsan, Republic of Korea

[3]School of Life Sciences, Ulsan National Institute of Science and Technology (UNIST), Ulsan, Republic of Korea

[4]Section of Cell and Developmental Biology, Division of Biological Sciences, University of California, San Diego, La Jolla, CA, USA

[5]Center for Computational Biology and Bioinformatics, University of California, San Diego, La Jolla, CA, USA

[6]Department of Pediatrics and Department of Computer Science and Engineering, University of California, San Diego, La Jolla, CA, USA

## Abstract

Haematopoietic stem and progenitor cells (HSPCs) have been the focus of developmental and regenerative studies, yet our understanding of the signalling events regulating their specification remains incomplete. We demonstrate that *supt16h*, a component of the Facilitates chromatin transcription (FACT) complex, is required for HSPC formation. Zebrafish *supt16h* mutants express reduced levels of Notch-signalling components, genes essential for HSPC development, due to abrogated transcription. Whereas global chromatin accessibility in *supt16h* mutants is not substantially altered, we observe a specific increase in *p53* accessibility, causing an accumulation of p53. We further demonstrate that p53 influences expression of the Polycomb-group protein PHC1, which functions as a transcriptional repressor of Notch genes. Suppression of *phc1* or its



✉**Correspondence and requests for materials** should be addressed to D.T. or Y.L., dtraver@ucsd.edu; yoonsunglee@ibs.re.kr.

Author contributions

Conceptualization and methodology: Y.L, D.Y. and D.T. Validation: Y.L and S.G.E. Formal analysis and visualization: S.G.E. Investigation: Y.L., S.G.E., H.S., E.R., A.S., E.-S.K., J.E.M., C.-K.O., C.B, U.S., S.G., Y.H.P., L.P., M.-S.K., S.K. and K.M. Software: S.G.E., D.S. and C.A.N. Writing of the original draft: S.G.E., Y.L., D.T., D.Y. and K.L.C. Supervision: Y.L. and D.T.

Competing interests

All authors declare no competing interests.

**Extended data** is available for this paper at https://doi.org/10.1038/s41556-020-00604-7.

**Supplementary information** is available for this paper at https://doi.org/10.1038/s41556-020-00604-7.

upstream regulator, *p53*, rescues the loss of both Notch and HSPC phenotypes in *supt16h* mutants. Our results highlight a relationship between *supt16h*, *p53* and *phc1* to specify HSPCs via modulation of Notch signalling.

Haematopoiesis is an evolutionarily conserved process that allows for a small population of haematopoietic stem and progenitor cells (HSPCs) to generate trillions of blood cells over a lifetime. Despite being one of the best characterized stem-cell systems, the ontogeny of HSPCs is not completely understood[1]. Many studies have focused on events required for HSPC emergence, whereby HSPCs bud from the dorsal aorta into circulation, but little is known about the previous signals needed to determine HSPC fate[2,3]. To fill these gaps in our understanding, we employed a forward genetic screen in zebrafish to detect genes required for HSPC specification and identified *supt16h*, a component of the Facilitates chromatin transcription (FACT) complex that forms a heterodimer with SSRP1. The FACT complex has been described in two roles: (1) a histone chaperone that promotes H2A-H2B dimer dissociation from the nucleosome, allowing RNA polymerase II (RNAP2) to access chromatin templates[4] and (2) an initiation and elongation factor that colocalizes with RNAP2 to allow for transcriptional activity[5,6].

Despite what might be considered a globally essential function in genome regulation, we found *supt16h* primarily affects the expression of Notch-pathway components essential for HSPC specification. An absence of Notch receptors (*notch1* and *notch3*) and ligands (*jagged1, deltaC* and *deltaD*) results in a loss of HSPCs in mouse and zebrafish[7–10]. Moreover, we demonstrated that these ‘Notch genes’, defined here as Notch receptors and ligands, are transcriptionally affected by the levels of polyhomeotic homologue 1 (PHC1), a Polycomb-group protein whose expression is controlled by p53. Although canonically described in the induction of apoptosis, cell-cycle arrest and senescence, recent findings show p53 involvement in genomic stability, transcriptional regulation and epigenetic modifications[11–13]. We demonstrate that p53 controls *phc1* expression through direct binding at the *phc1* locus, which influences transcriptional repression of Notch genes. This work highlights a previously uncharacterized method of Notch-gene regulation and elucidates an unrecognized relationship between Polycomb-group proteins, p53 and FACT in modulating Notch-gene transcription during HSPC development.

## Results

### A forward genetic screen identifies *supt16h*$^{-/-}$ mutants lacking HSPCs.

Zebrafish *supt16h* mutants (*supt16h*$^{-/-}$) were obtained through a forward genetic screen for animals defective in HSPC specification (Extended Data Fig. 1a) and identified using RNA sequencing (RNA-seq)-based single nucleotide polymorphism (SNP) linkage mapping[14]. Our candidate gene mapped to Chromosome 7 and corresponded to a premature stop codon in *supt16h* (Extended Data Fig. 1b–d and Supplementary Table 1). Mutants exhibited enlarged hindbrains and curved tails beginning at 32 h post fertilization (h.p.f.), leading to lethality at 3 d post fertilization (Fig. 1a,b). These traits were linked to a complete loss of HSPCs, as assessed by whole-mount in situ hybridization (WISH) for *runx1* and *cmyb* HSPC markers along the aortic floor at 28 and 36 h.p.f., respectively, as well as RNA-seq

and quantitative reverse transcription PCR (RT-qPCR) analyses (Fig. 1c–f and Extended Data Fig. 1e,f). In addition, *supt16h*$^{-/-}$ mutants on a Tg(*cmyb:eGFP; kdrl;mCherry*) background, where double-positive cells along the aortic floor represent HSPCs, exhibited a significantly reduced number of HSPCs compared with their wild-type (WT) siblings (Fig. 1g–i)[2]. Moreover, injection of WT *supt16h* messenger RNA into mutant embryos rescued the hindbrain, tail and HSPC phenotypes (Fig. 1j–q), and injecting *supt16h* antisense Morpholino oligonucleotide (MO) phenocopied the reduced HSPCs in *supt16h*$^{-/-}$ mutants (Extended Data Fig. 1g–m)[2]. Together, these data indicate that Supt16h is required for HSPC formation.

The *supt16h* gene was broadly expressed throughout development (Extended Data Fig. 2a–c and Fig. 1r). Higher-magnification and cross-sectional views of *supt16h* WISH embryos showed its expression along the dorsal aorta floor, where HSPCs emerge (Fig. 1s–u and Extended Data Fig. 2d,e). Moreover, RT-qPCR of HSPCs purified using fluorescence-activated cell sorting (FACS) demonstrated enrichment of *supt16h*, providing further evidence of expression in HSPCs. In addition, the transcription of *supt16h* was substantially reduced in our mutant line—as observed by WISH, RNA-seq and RT-qPCR—due to nonsense-mediated decay (Fig. 1v–z and Extended Data Fig. 2f–k). To further characterize the specific requirement of *supt16h* on HSPC formation, we examined tissues essential for HSPC specification. The expression of markers of the posterior lateral mesoderm, somites, sclerotome, vascular endothelium, dorsal aorta, vein, primitive erythrocytes and primitive leukocytes was normal in mutants (Extended Data Fig. 2f–t). Overall, these results indicate that the specific loss of HSPCs in *supt16h*$^{-/-}$ is not due to improper formation of upstream or adjacent tissues.

## The Notch pathway is downregulated in *supt16h*$^{-/-}$.

To explore the contribution of *supt16h* during haematopoiesis, we performed Gene Ontology (GO) analysis using transcripts that were significantly downregulated in mutants (Extended Data Fig. 3a,b)[15,16]. Although the molecular processes that were most affected were associated with transcriptional regulation and binding of RNAP2 to DNA, we observed no bias in the number of upregulated and downregulated genes in *supt16h*$^{-/-}$ (Extended Data Fig. 3c). We did observe that the only affected signalling pathway and top downregulated biological process was Notch (Fig. 2a and Extended Data Fig. 3b), which has been associated with HSPC specification and emergence[7–9,17–21]. The transcriptional levels of Notch genes were reduced in mutant embryos at 28–32 h.p.f., based on RNA-seq, RT-qPCR and WISH analyses (Fig. 2b–g and Extended Data Fig. 3d–g). The *notch2* gene was reduced to a lesser extent, but it is known to be dispensable for HSPC formation[7,22]. Furthermore, mutants harbouring the Notch reporter line *Tp1:GFP* displayed significantly downregulated Notch activity in the dorsal aorta at 22 and 28 h.p.f. (Fig. 2h–j and Extended Data Fig. 3h–j). Sorted *Tp1:GFP*$^{+}$;*fli1:DsRed*$^{+}$ cells, which have been shown to have high *runx1* expression, were present at lower levels in *supt16h* morphants[21] (Extended Data Fig. 3k,l). Interestingly, there was no alteration on Notch-gene activity in mutants during early somitogenesis at 14 h.p.f. (Extended Data Fig. 3m,n). Therefore, *supt16h*$^{-/-}$ mutants have impaired late (28 h.p.f.), but not early (14 h.p.f.), Notch-gene expression. To determine whether the reduction in Notch-gene transcripts in *supt16h*$^{-/-}$ mutants led to HSPC loss, we forced global

expression of Notch intracellular domain 1 (NICD) using a Tg(*hsp70*) driver and endothelial expression using a Tg(*cdh5:gal4ff*) driver[23]. Restoration of Notch activity using these transgenes in *supt16h*$^{-/-}$ mutants rescued HSPC development (Fig. 2k–r and Extended Data Fig. 3o–v). Together, these data indicate that Notch signalling is downstream of *supt16h* function during HSPC specification.

## Induction of p53 in *supt16h*$^{-/-}$ mutants perturbs HSPC formation.

The FACT complex colocalizes with RNAP2 to initiate transcription and can associate with Tif1γ to promote transcriptional elongation of erythroid genes[24]. We therefore examined the connection between Supt16h and initiation and elongation of Notch-gene transcripts using RT-qPCR, assaying for changes between the 3'-and 5'-end transcript levels. We found that, although transcriptional initiation was substantially altered in all but three Notch genes, elongation of *supt16h*$^{-/-}$ transcripts was unaffected in most genes, which suggests that the Notch genes are inefficiently transcribed as a result of aberrant Supt16h activity as part of the transcriptional initiation complex (Extended Data Fig. 4a).

Due to the role of Supt16h as a histone chaperone to remodel chromatin, we conducted an assay for transposases accessible chromatin with sequencing (ATAC-seq) to determine whether chromatin accessibility of the Notch-gene coding sequences was affected in the *supt16h*$^{-/-}$ mutants. We observed no difference in accessibility at transcriptional start sites or on Notch genes globally, and no correlation between DNA accessibility and Notch transcription (Extended Data Fig. 4b–g). As there was no obvious connection between Notch-gene transcription levels and accessibility, we evaluated genes with the most differentially accessible peaks in the *supt16h*$^{-/-}$ mutants and found *p53* to be the most accessible gene (Fig. 3a and Extended Data Fig. 4h). We observed notable increases in both *p53* transcript and protein expression in mutants (Fig. 3b–d and Extended Data Fig. 4i,j). WISH analyses demonstrated *p53* increases throughout *supt16h*$^{-/-}$ embryos, including the dorsal aorta, commencing at 18 h.p.f. (Fig. 3e–j and Extended Data Fig. 4k–r). To determine whether there is a specific haematopoietic consequence of reducing the levels of *p53* in the absence of Supt16h, we examined *supt16h*$^{-/-}$ crossed with *p53* mutants (*tp53*$^{zdf1/zdf1}$)[25]. The *supt16h;p53* double mutants rescued HSPC formation, probably due to an inability of p53 to activate the downstream targets (Fig. 3k–m)[25]. Morpholino oligonucleotide knockdown of *supt16h* in the *p53* mutants or *p53* in the *supt16h*$^{-/-}$ mutants similarly rescued HSpCs (Fig. 3n–q and Extended Data Fig. 3s–v). This was further highlighted by RT-qPCR, where we detected a significant increase in *runx1* transcripts in the *p53*-MO-injected mutants (Fig. 3r).

To examine whether a reduction in *p53* prevents HSPC death to rescue specification in *supt16h*$^{-/-}$ mutants, we conducted terminal deoxynucleotidyl transferase dUTP nick-end labelling (TUNEL) assays and acridine orange staining on *supt16h*$^{-/-}$ embryos harbouring a *fli1:GFP* endothelial reporter that marks the shared vascular precursors of HSPCs. We discerned no difference in the number of double-positive TUNEL$^{+}$*fli1*$^{+}$ cells at 14, 18 and 28 h.p.f., despite being able to distinguish between global apoptotic events in WT and mutants from 18 h.p.f. (Fig. 3s–w and Extended Data Fig. 5a–r). This demonstrates that a loss of HSPCs in *supt16h*$^{-/-}$ mutants is not a result of their death in the endothelium. We

further characterized the role of p53-independent apoptosis and found that p53 loss in the *supt16h*$^{-/-}$ mutants did not resolve their abnormal morphologies or extend survival (Extended Data Fig. 5s–w). In addition, we observed that although general genotoxic stress through ionizing radiation increased *p53* expression and cell death, it did not affect HSPC specification (Extended Data Fig. 5x–e'). Overall, these results suggest that elevated *p53*, caused by a global loss of *supt16h*, perturbs HSPC formation independent of cell-mediated apoptosis.

## The transcription levels of the Notch genes are influenced by *p53* abundance.

It is known that p53 is a transcriptional regulator of numerous genes by direct stimulation of the transcription of RNAP2-transcribed genes or activation of the associated pathways[13]. To address whether ectopically elevated p53 is related to the reduced transcript levels of Notch genes in *supt16h*$^{-/-}$ mutants, we examined the effect of *p53* downregulation on Notch-pathway activation using the *Tp1:GFP* Notch reporter line and found that *p53*-MO injection into *supt16h*$^{-/-}$ mutants restored Notch activity (Fig. 4a–e). Both double mutants and double morphants of *supt16h;p53* also rescued *notch1b*, which we previously demonstrated is required for HSPC specification, and *runx1* expression (Fig. 4f–m and Extended Data Fig. 6a–h)[8]. We next tested the effect of differences in p53 levels on Notch-gene transcription, given that previous studies have linked p53 abundance to impaired RNAP2 activity and suppressed mRNA synthesis[26,27]. We observed reduced expression of *p21* —a downstream target of p53—in *supt16h*$^{-/-}$ mutants (WT, heterozygous and homozygous for *p53*), which was relative to the genetic dosing of the *p53* mutants (Fig. 4n). Remarkably, we observed the converse trend with *runx1* and Notch genes, where the transcript levels increased following p53 reduction (Fig. 4o,p). These data indicate that p53 and Supt16h coordinate to activate the transcription of Notch genes during HSPC specification.

To further examine the epistasis between p53 and Notch signalling during HSPC formation, we co-injected *notch1b*- and *p53*-MOs to determine whether *p53* regulation of Notch genes is confined to *supt16h*$^{-/-}$. We observed an absence of HSPCs in *notch1b* morphants and, notably, a lack of HSPC rescue in double *notch1b; p53* morphants (Extended Data Fig. 6i–l). In addition, *p53* knockdown in *mindbomb (mib)* mutants with defective Notch-pathway signalling and HSPC formation resulted in continued aberrant HSPCs (Extended Data Fig. 6m–t)[28]. These data indicate that a reduction of p53 alone is not sufficient to restore HSPCs in embryos when Notch genes are downregulated and further suggests that Notch signalling is downstream of *p53* function.

## HSPC specification is unaffected by *ssrp1*.

As part of the larger FACT complex, Supt16h forms a heterodimer with SSRP1 to effectively alter chromatin accessibility[29]. We examined the consequences of *ssrp1* knockdown on HSPC formation to address whether the effect of Supt16h on HSPC development was independent of the FACT complex or associated with the role of FACT as a transcriptional regulator. Given that the zebrafish paralogue *ssrp1a* can compensate for the role of *ssrp1b*[30,31], we mainly focused on *ssrp1a* in future experiments. HSPC development was normal in both single *sspr1a* and double *ssrp1a; ssrp1b* morphants (Fig. 5a–h). Similar results were observed for *ssrp1a*$^{-/-}$, characterized by a premature stop codon on exon 11 and

reduced *ssrp1a* transcripts (Fig. 5i–k)[32]. In addition, we observed no effect on the dorsal aorta, early red blood cell or vasculature in morphants (Extended Data Fig. 7a–f). WISH analysis showed both *ssrp1a* and *ssrp1b* maintained a similar global expression pattern to *supt16h* from 14 to 32 h.p.f., and that these genes are present along the floor of the dorsal aorta, which corresponded to their detectable upregulation in HSPCs (Fig. 5l–p and Extended Data Fig. 8g–o).

To further understand of the disparate effect of SSRP1 and Supt16h on HSPC development, we examined the influence of SSRP1 on p53 and Notch abundance. We saw no discernable difference in *p53* expression or cell-death events in the *ssrp1a* mutants or morphants (Fig. 5q and Extended Data Fig. 8p–x). Furthermore, we observed no altered Notch signalling activity in our morphants following *ssrp1a* knockdown in the *Tp1:GFP* reporter line (Fig. 5r,s and Extended Data Fig. 8y). Consistent with these findings, *notch1b* expression was unchanged in both *ssrp1a* mutants and morphants based on WISH (Fig. 5t,u and Extended Data Fig. 8z,a'). Overall, these results demonstrate that, despite sharing similar expression profiles to *supt16h, ssrp1a* is dispensable for proper Notch activity, p53 activation and HSPC formation, thereby suggesting that Supt16h and SSRP1 maintain independent roles during HSPC specification.

## p53 regulates *phc1* expression to control Notch-gene transcription and HSPC specification.

To assess the mechanism by which p53 regulates Notch-gene expression in *supt16h*$^{-/-}$ mutants, we conducted chromatin immunoprecipitation-sequencing (ChIP-seq) to investigate whether p53 binds directly to Notch genes to influence their activity or to known transcriptional regulators to indirectly affect Notch expression. Following p53-based ChIP-seq, we observed through GO analysis that the most highly expressed genes were associated with apoptotic processes and p53 signalling, including *p21* expression (Extended Data Fig. 8a–c). We then examined the direct interaction between p53 and Notch genes, and found no substantial increase in binding in *supt16h*$^{-/-}$ mutants (Extended Data Fig. 8d–f), indicating that p53 does not mediate Notch-gene expression directly.

We thus explored the option that p53 indirectly influences Notch signalling by increasing the expression of a Notch transcriptional repressor, given that correlative analysis of our ChIP-seq results with our RNA- and ATAC-seq datasets showed a majority of the ChIP genes that were differentially expressed were upregulated and highly accessible (Extended Data Fig. 8g,h). We discovered a known Notch transcriptional repressor, *phc1*, had elevated p53 binding and increased accessibility in *supt16h*$^{-/-}$ mutants (Fig. 6a,b). In addition, we observed elevated *phc1* expression in *supt16h* mutants and morphants, paralleling the upregulation of *p53* levels to suggest p53 enhances the expression of *phc1* in these embryos (Fig. 6c–f and Extended Data Fig. 8i–w). To further determine transcriptional regulation of *phc1* by p53, we performed a luciferase enhancer assay[33] in HCT116 p53-knockout cells using a 611-base pair intronic sequence of zebrafish *phc1* based on p53 ChIP binding and a deletion of the 20-base pair p53 responsive element[34] (Δp53 RE) found in this sequence (Fig. 6g). We observed a notable increase in luciferase activity at the *phc1* intron sequence compared with the controls and Δp53 RE mutants, whereas no change in luciferase activity

was observed in the absence of p53 (Fig. 6h,i), suggesting that p53 has the ability to regulate *phc1* transcription.

We knocked down *phc1* in *supt16h*$^{-/-}$; *Tp1:GFP* mutants to determine the effect of *phc1* on Notch expression and HSPC formation, and observed a detectable elevation in Notch activity at 28 h.p.f. (Fig. 7a–d). We obtained similar results through WISH, where *notch1b, notch3, dlc* and *dll4* expression along with the HSPC maker *runx1* were rescued specifically within the dorsal aorta in *supt16h*$^{-/-}$ mutants injected with phc1-MO (Fig. 7e–x). However, the rescue was not as pronounced in *notch1a, dla* and *dld*, whose expression pattern was contained mostly to neural tissues (Extended Data Fig. 9a–l). In addition, we performed complementary experiments overexpressing *phc1* via injection of mRNA or plasmid containing endothelial-specific *fli1a* promoter driving *phc1* and found no pronounced decrease in Notch transcripts or effect on HSPC formation with sole induction of *phc1* expression in WT embryos (Extended Data Fig. 9m–j'). These data highlight the ability of p53 to modulate *phc1* expression and suggest PHC1 influences specific Notch genes, notably those expressed along the dorsal aorta—such as *notch1b, notch3, dlc* and *dll4*—to affect HSPC formation.

## Discussion

We report the characterization of a *supt16h* vertebrate mutant, highlighting the complex mechanism by which the Notch pathway is regulated to control HSPC development. Our findings have several implications, notably: (1) a histone chaperone plays an essential role in haematopoietic development, (2) vertebrate Supt16h functions as a transcriptional regulator but not as a global chromatin remodeller, (3) Supt16h has independent roles from SSRP1 and the FACT complex, (4) p53 can mediate cell differentiation and stem-cell fate through specific gene activation, and (5) PHC1 influences the transcription of Notch genes to allow HSPC formation. Ultimately, our study has elucidated a highly precise and complex mechanism for the regulation of the expression of Notch gene components.

We suggest a model to describe this complex regulation where in a WT setting, *p53* and *phc1* exhibit baseline levels of accessibility and expression that result in normal transcription of Notch genes and proper HSPC specification (Extended Data Fig. 10). In the absence of *supt16h*, the *p53* locus becomes highly accessible, resulting in elevated *p53* levels. Subsequently, p53 binds to *phc1* chromatin to allow for enhanced *phc1* expression. PHC1, as part of the Polycomb repressive complex 1 (PRC1), then inhibits Notch signalling by acting as a transcriptional repressor or co-repressor of Notch genes. Due to the absence of Notch expression, HSPCs fail to specify.

Notch has multiple iterative roles during HSPC development[3,7–9,17,21,35]. Here, we propose that the levels of *p53*, through Supt16h-mediated accessibility, influence the transcriptional abundance of Notch genes by activating *phc1* expression. PHC1 influences Notch-gene expression as part of PRC1, possibly as a co-factor with another protein based on our knockdown and overexpression studies. Research by Martinez and colleagues support the role of the Ph locus as a direct Notch transcriptional regulator with their studies in *Drosophila* showing that knockout of the Ph locus (*ph-p* and *pd-d*) upregulates Notch genes

(*notch, serrate* and *eyegone*), whereas overexpression reduces expression[36]. Similar work by Boyer and colleagues demonstrate Phc1 binds to *dll4* and *dll1* along with 920 other genes in mouse ES cells to influence differentiation through dynamic repression[37]. Additional studies, both in *Drosophila* and human cell lines, have shown that many target genes of Polycomb-group proteins are components of the Notch signal-transduction pathway[38–40].

An alternative possibility is that PHC1, as part of PRC1, regulates HSPC formation independently of Notch signalling by instead binding to core transcription factors that affect HSPC expression. Yu and colleagues demonstrated two core PRC1 components, Bmi1 and Ring1b, directly bind to the Runx1-CBFβ transcription factor complex, which is highly involved in haematopoietic development. Following knockdown of Bmi1 or Ring1b, zebrafish HSPC formation was markedly impaired, highlighting the necessary recruitment of PRC1 by Runx1-CBFβ to affect haematopoiesis. Moreover, studies of *phc1*-deficient mice show impaired haematopoietic activity in the fetal liver due to its role in maintaining HSPC self-renewal and proliferation capabilities[41,42]. Cumulatively, these data implicate a role of PRC1 regulation during HSPC formation.

The influence of Supt16h on *p53* expression has been highlighted in several studies that link FACT to p53 activation in response to DNA damage[43,44]. On forming a complex with FACT, the protein kinase CK2 undergoes a conformational change that allows it to preferentially recognize and activate p53 (ref. [44]). In addition, drug-induced ‘chromatin trapping’ of the FACT complex by curaxin in tumour lines results in p53 pathway activation, NF-κB suppression and tumour-cell death[45]. Further work is required to determine the mechanism by which Supt16h influences *p53* expression, whether it is through transcriptional regulation, as we have suggested based on *p53* chromatin accessibility, or through a direct protein interaction with FACT, based on the work of Keller and colleagues[43,44].

Despite being characterized as a histone chaperone, global chromatin accessibility was not substantially affected in *supt16h*$^{-/-}$ embryos. This could be attributed to the heterogeneity of using whole embryos, which makes it difficult to accurately assess global impacts, especially when transcriptional changes may be more subtle in certain tissues. Kolundzic and colleagues have compelling studies on FACT in more homogenous systems, suggesting accessibility correlates with gene expression[46]. In addition, they have shown in *C. elegans* and human fibroblasts that FACT can both positively and negatively influence gene regulation and it does not notably alter chromatin accessibility genome wide, which provides support for our observation in zebrafish. Other studies have shown FACT increases chromatin accessibility in certain regions or only changes DNA shape in a weak and transient manner, which parallels the minor changes we observed in the chromatin accessibility and tissue-specific alteration of Notch transcription in *supt16h*$^{-/-}$ animals[47]. Further research on the temporal and tissue-specific function of Supt16h, using our vertebrate animal model, can expand our understanding of the highly complex and tightly regulated role of the FACT complex during gene regulation.

## Online content

Any methods, additional references, Nature Research reporting summaries, source data, extended data, supplementary information, acknowledgements, peer review information; details of author contributions and competing interests; and statements of data and code availability are available at https://doi.org/10.1038/s41556-020-00604-7.

## Methods

### Zebrafish strains.

Zebrafish were maintained and propagated as previously described[48] in accordance with the guidelines of the University of California, San Diego Institutional Animal Care and Use Committee (IACUC). Embryos and adult fish were raised in a circulating aquarium system (Aquaneering) at 28 °C. The following lines were used: WT AB*, WT WIK, Tg(*cmyb:GFP*)$^{zf169}$ (ref. [49]), Tg(*kdrl:mCherry*) (ref. [18]), Tg(*fli1:DsRed*)$^{um13}$ (ref. [50]), Tg(*CD41:GFP*) (ref. [51]), Tg(*Tp1:GFP*)$^{um14}$ (ref. [52]), UAS:*NICD-myc* Tg(5×*UAE-E1b:6×MYC-notch1a*)$^{kca3}$ (ref. [17]), TgBAC(*cdh:gal4ff*)$^{mu101}$ (ref. [53]), Tg(*hsp70l:gal4*)$^{1.5kca4}$ (ref. [54]), Tg(*fli1a:GFP*)$^{Y1}$ (ref. [55]), *tp*53$^{zdf1/zdf1}$ (ref. [25]) and *ssrp1a*$^{sa31984}$ (ref. [32]). Mutant *supt16h* animals were generated through a forward genetic screen described in the ‘ Forward genetic screen’ section of Methods. The allele number for *supt16h*$^{-/-}$ zebrafish is SD45. Heat shock was performed at 14 h.p.f. for 45 min at 37 °C as previously described[17]. Details on the strains and ages are noted for each experiment. Gender was not selected in any of the studies conducted.

### Forward genetic screen.

Wild-type AB* strain males were mutagenized through treatment with 3.3 mM ENU (Sigma) weekly for three weeks. The mutagenized males were crossed to WT WIK females to produce the $F_1$ generation. These were outcrossed to WIK or AB animals and the resulting $F_2$ siblings were subjected to random sibling incrosses. The $F_3$ embryos were screened using WISH at 26–30 h.p.f. with the *runx1* HSPC marker.

### Mutant mapping and differential expression analysis by RNA-seq.

Approximately 40 *supt16h*$^{-/-}$ and 40 WT embryos were collected at 32 h.p.f. and RNA was extracted using TRIzol (Ambion). RNA libraries were generated using a TruSeq stranded mRNA kit and run on an Illumina HiSeq2500 PE50 system. The RNA-seq data underwent quality assessments using FastQC 0.11.2 and MultiQC 1.5 and were trimmed using Trimmomatic 0.32 (refs. [56,57]). Reads were aligned to the zebrafish genome Zv9.69 and the assembled transcripts were inputted into the RNAmapper pipeline to map the mutants through linkage analysis of SNP haplotype blocks. Candidate mutations were identified using the Ensembl Variant Effect Predictor[14]. A list of candidate SNPs causal for the mutation was then generated using the RNAidentifie.R custom R script[14].

Three additional biological replicates to assess differential expression were sequenced on the Illumina NovaSeq PE100 system. Quality-control checks were performed using RSeQC[58] and FastQC[56]. The reads were aligned using the Burrows-Wheeler transform[59], and aligned

with TopHat[60]. Cufflinks was used to determine differential expression and the DEGseq R package was used to identify genes that were differentially expressed[61].

### WISH.

Embryos were fixed overnight in 4% paraformaldehyde (PFA) in PBS at 4 °C, washed with PBS containing 0.1% Tween-20 (PBST) and transferred stepwise into methanol in PBST (25, 50, 75 and 100%). The embryos were hydrated stepwise into PBST (25, 50, 75 and 100%) and incubated with 100% acetone at −20 °C for 10 min for embryos at 10–32 h.p.f. and 15 min for older embryos. The samples were washed with PBST, prehybridized at 65 °C for 1 h in hybridization buffer (Hyb; 50% formamide, 5×SSC, 500 μg $ml^{-1}$ torula (yeast) tRNA, 50 μg $ml^{-1}$ heparin, 0.1% Tween-20 and 9 mM citric acid (pH 6.5)) and hybridized overnight with digoxigenin (DIG)- or fluorescein-labelled RNA probe in Hyb. The samples were washed stepwise at 65 °C for 15 min in Hyb containing a 2×SSC mix (75, 50 and 25%), followed by two washes with 0.2×SSC for 30 min at 65 °C. Subsequent washes were performed at room temperature for 5 min with 0.2×SSC in PBST (75%, 50%, 25%). The embryos were placed in PBST containing WISH block solution (2% heat-inactivated goat serum and 2 mg $ml^{-1}$ BSA) for 1 h and incubated overnight at 4 °C in anti-DIG-AP (1:5,000; Roche) diluted in WISH block solution. To visualize, the samples were washed 3× in AP (alkaline phosphatase) reaction buffer (100 mM Tris, pH 9.5, 50 mM $MgCl_2$, 100 mM NaCl, 0.1% Tween-20 and 1 mM tetramisole hydrochloride) for 5 min and incubated in AP reaction buffer with NBT/BCIP substrate (Promega).

Antisense RNA probes for the following genes were prepared using DIG- or FITC-labelled UTP (Roche) as previously described: *cdh5*, *cmyb*, *dla*, *dlb*, *dlc*, *dld*, *dll4*, *efnb2a*, *etsrp*, *flt4*, *foxc1b*, *gata1*, *jag1a*, *kdrl*, *l-plastin*, *lmo2*, *notch1a*, *notch1b*, *notch2*, *notch3*, *rag1*, *runx1*, *scl* and *twist1b*[62,63]. The probes for *phc1, sspr1a, ssrp1b* and *supt16h* were generated from the full-length complementary DNA.

### Immunohistochemistry.

For staining of Myc in *UAS:NICD-myc* after WISH, the samples were placed in block solution (150 mM maleic acid, pH 7.5, 100 mM NaCl and 2% Boehringer blocking reagent) for 1 h at room temperature and incubated with anti-c-myc antibody (1:1,000; BioLegend) in block solution overnight at 4°C. These were washed 4× with block solution at room temperature for 30 min, incubated with secondary donkey anti-mouse AlexaFlour-488 antibody (1:1,000; ThermoFisher) at 4 °C overnight and washed 4× with blocking solution at room temperature for 30 min.

### Double fluorescence in situ hybridization.

Double fluorescence in situ hybridization embryos were fixed with 4% PFA, dehydrated and rehydrated as described earlier for WISH. The embryos were then washed twice with PBST for 5 min, fixed again with 4% PFA for 20 min at room temperature, digested with Proteinase K (Sigma) for 3 min at room temperature, rinsed with PBST and fixed again with 4% PFA for 20 min at room temperature. These were then washed twice with PBST, incubated in Hyb buffer at 65 °C for 1 h, and incubated with anti-DIG *gfp* and anti-FITC *etsrp* probes diluted in Hyb at 65 °C for 2 d. After incubation, the following washes were

performed at 65 °C: twice with Hyb for 30 min, twice with SSC for 15 min and once with 0.2×SSC for 30 min. The embryos were incubated in block solution (150 mM maleic acid, pH 7.5, 100 mM NaCl and 2% Boehringer blocking reagent) for 1 h at room temperature. Diluted anti-flourescein-POD (1:500; Roche) in block solution was then added overnight at 4 °C. The following washes were performed at room temperature: 4× with maleic acid buffer (150 mM maleic acid, pH 7.5 and 100 mM NaCl) for 20 min and 2× with PBS for 5 min. The samples were incubated for 1 h in TSA plus flourescein solution (PerkinElmer), dehydrated stepwise into methanol in PBS (30, 50, 75 and 100%), incubated in 2% $H_2O_2$ in methanol for 30 min and rehydrated into methanol in PBS (75, 50 and 30%). The embryos were washed 2× with PBS, fixed with 4% PFA for 20 min, washed 2× with PBS, blocked for 1 h at room temperature with blocking solution and incubated with anti-DIG-POD (1:1,000; Roche) overnight at 4 °C. The following washes were then done at room temperature: 4× with maleic acid buffer for 20 min and 2× with PBS for 5 min. The samples were incubated for 1 h in TSA plus Cy5 solution (PerkinElmer), washed 3X with PBST, fixed with 4% PFA at room temperature and placed stepwise in glycerol (25 and 50%).

### Western blotting.

Approximately 400 WT and 400 *supt16h*-mutant sibling embryos were deyolked (manual pipetting) at 32 h.p.f. in Ginzburg fish Ringer solution (55 mM NaCl, 1.8 mM KCl and 1.25 mM $NaHCO_3$). Whole-cell lysates were prepared by lysing the cells with Buffer X (100 mM Tris-HCl, pH 8.5, 250 mM NaCl, 1 mM EDTA, 1% Nonidet P-40 and 5 mM $MgCl_2$) with PhosSTOP phosphatase inhibitor (Roche), complete EDTA-free protease inhibitor cocktail (Roche) and 500 units of benzonase for 1 h at 4 °C. The digested lysates were sonicated at 80% amplitude for 3 min (3 s on, 3 s off) and centrifuged at 13,000*g* for 5 min at 4 °C. The collected supernatant was measured using a Bradford assay. Approximately 20 μg of protein was boiled for 3 min at 100 °C, loaded onto a 7.5% SDS-PAGE gel and transferred onto a nitrocellulose membrane. The membrane was blocked (5% milk) and probed with anti-Supt16h (1:500; Cell Signaling Technology), anti-P53 (1:500; GeneTex), anti-α-tubulin (1:20,000; Sigma Aldrich) or anti-Lamin B1 antibody (1:2,000; Abcam) in TBST. Amersham ECL anti-mouse IgG (horseradish peroxidase-linked; 1:5,000; GE Healthcare) and Amersham ECL anti-rabbit IgG (horseradish peroxidase-linked; 1:5,000; GE Healthcare) secondary antibody was used. Protein was detected using Supersignal west pico luminol/enhancer solution (ThermoFisher) and Supersignal west femto maximum sensitivity substrate (ThermoFisher). Images were taken on a ChemiDoc XRS+ system using Image Lab (Bio-Rad).

### GO analysis.

The Gene Ontology Consortium's GO enrichment analysis (PANTHER classification system)[15,16] was used to perform GO analysis. Downregulated genes with a $\log_2$[fold change] > 1.0 based on Cufflinks were used for analysis of the RNA-seq data. Significant (adjusted $P > 0.05$) p53 ChIP peaks based on DESeq2 were used to analyse the ChIP-seq data.

### Microscopy and image analysis.

An SP5 inverted confocal microscope (Leica Microsystems) was used to image fluorescent transgenic embryos, double fluorescence in situ hybridization and TUNEL assays. Fluorescein and GFP were excited by a 488-nm laser, DsRed and Cy3 by a 543-nm laser, Strepavidin-647 by a 633-nm laser and 4,6-diamidino-2-phenylindole (DAPI) by a 405-nm laser. Sequential images were overlaid using ImageJ (NIH) or Imaris (Bitplane). A Zeiss AxioZoom.V16 microscope was used to image the immunohistochemistry samples using the AxioVision software 4.8. Visible-light imaging for sections or WISH was performed on a BX-51 Olympus or Leica MZ16 microscope (Leica FireCam Software 3.4.1).

### Microinjections of mRNA, Morpholino and plasmid.

Embryos were injected at the one-cell stage with 1 nl of antisense MOs (GeneTools) and/or mRNA. The MOs were diluted from 25 mM stocks in DEPC-treated $H_2O$ and were used at concentrations of 2.5 ng *supt16h*-MO[24], 3.75 ng *p53*-MO[64], 2.5 ng *ssrp1a*-MO[31], 2.5 ng *ssrp1b*-MO[31] and 2.5 ng *phc1*-MO-5′-GGCTTTCTGACCCACCTGAACAG-3′. Capped mRNAs were synthesized from linearized pCS2+ constructs using an mMessage mMachine SP6 transcription kit (Ambion). Full-length *supt16h* or *phc1* mRNA was injected into embryos at 200 ng $\mu l^{-1}$ and 100 ng $\mu l^{-1}$, respectively. Transient *phc1* expression was conducted using the 478 p5Efli1ep plasmid (Addgene, 31160), described here as *fliep:phc1.* A PM1000 cell microinjector (MicroData Instrument) was used to inject the embryos using borosilicate glass needles (Sutter Instrument) made on the PMP102 micropipette puller (MicroData Instrument).

### Cell preparation and flow cytometry.

Tg(*CD41:GFP; kdrl:mCherry)* embryos ($n$ = 100–200) were collected at 48 h.p.f., dissociated and digested with 1×Liberase TM (Roche) in PBS at 32 °C for 30 min. Cells were centrifuged at 300xg at 4 °C for 10 min and resuspended in PBSF (1% heat-inactivated fetal bovine serum). The cells were filtered through a 40-μm filter by centrifugation and washed with PBSF. SYTOX red (ThermoFisher) was added to exclude the non-viable cells. Sorting was performed on a FACSAria II (BD Biosciences).

Tg(*fli1a:dsRed; TP1:eGFP*) embryos *(n* = 100–200) were dissociated at 22 h.p.f., with shaking at 120 r.p.m. in dissociation buffer (0.9×PBS, Liberase TM (1:50; Roche) and 10 μM EDTA) at 37 °C for 1–2 h. Cells were pelleted at 500g for 5 min, resuspended in buffer (0.9×PBS, 1% FBS, 1 mM EDTA and 0.1 μg $ml^{-1}$ DAPI) and filtered through an 80-μm filter. The cells were quantified using a BD LSR Fortessa and analysed using FlowJo. DAPI was used for dead-cell discrimination; 3–5 × $10^6$ cells were analysed per biological replicate.

### RT-qPCR.

RNA was extracted from whole embryos using TRIzol (Ambion) or an RNeasy mini kit (Qiagen). Complementary DNA was synthesized using an iScript gDNA clear cDNA synthesis kit (Bio-Rad). RT-qPCR was performed on a Bio-Rad CFX96 system according to the manufacturer's instructions. *Tbp* expression was used to normalize the amount of the investigated transcripts using $\Delta\Delta C_t$. The primers are listed in Supplementary Table 2.

### ATAC-seq.

Embryos were collected at 32 h.p.f. and deyolked in Ginzburg fish Ringer solution. Cells ($n$ = 50,000) were collected, washed with PBS and pelleted at 500 × $g$ for 5 min at 4 °C. Nuclei were extracted by adding 50 µl of cold lysis buffer (10 mM Tris-HCl, pH 7.4, 10 mM NaCl, 3 mM $MgCl_2$ and 0.1% (vol/vol) Igepal CA-630) and centrifuging at 500 × $g$ for 10 min at 4 °C. The pellets were resuspended in 50 µl transposition reaction (Nextera Tn5 transposase kit). The nuclei were incubated at 37 °C for 30 min and DNA was purified using an Omega MicroElute DNA cleanup kit. The DNA was PCR amplified and barcoded with NEBNext high-fidelity 2XPCR master mix using the following protocol: (1) 72 °C for 5 min, (2) 98 °C for 30 s, (3) 98 °C for 10 s, (4) 63 °C for 30 s, (5) 72 °C for 1 min, (6) five repeats of steps (3)-(5), and (6) hold at 4 °C (ref. [65]). RT-qPCR was performed to determine additional cycles. Libraries were size selected using Mag-Bind RxnPure plus (Omega), with the first selection eliminating the small products (0.4:1 ratio) and the second selection (1.4:1 ratio) to select the desired products. The samples were quantified using a BioAnalyzer and KAPA library quantification kit before sequencing at PE100 on a HiSeq4000 system (Illumina).

Two technical and three biological replicates were performed for the WT and *supt16h*$^{-/-}$ embryos. OLego 1.1.5 was used for sequence alignment[66] on the zebrafish genome GRCz10 and HOMER 4.9.1 was used to call and analyse the peaks[67]. The peaks were visualized using Integrative Genomics Viewer (IGV) 2.3.65 (ref. [68]).

### Genotyping.

DNA was extracted from embryos or fin clips by digesting with DNA extraction buffer (25 mM NaOH and 0.2 mM EDTA) for 1 h at 95 °C and stopped with Neutralization buffer (40 mM Tris-HCl). Genomic DNA was amplified by PCR using the primers: Supt16h-F, 5′-ATGAAGACGAGGACGAGGAA-3′ and Supt16h-R, 5′-TTATGTGGGTCGGGAACACT-3′ or Ssrp1a-F, 5′-TTGTCTGCAGCACCTTGTCA-3′ and Ssrp1a-R, 5′-TTTGGCTGCTGGGAATTTGT-3′. The amplified products were submitted for sequencing for SNP detection.

### Cryosection.

Following WISH, the embryos were washed with PBST and placed overnight in 30% sucrose at 4 °C. The samples were equilibrated 1:1 with Tissue Tek O.C.T. medium (Sakura) for 30 min at room temperature, mounted on cryoblocks containing O.C.T., and frozen on dry ice. Sections (7 µM) were cut on a Leica CM1860 Cryostat.

### Detection of apoptotic cell death by TUNEL labelling.

TUNEL was performed on rehydrated, fixed embryos that were permeabilized with PBSTx + dimethylsulfoxide (1×PBS, 0.5% Triton-X100 and 1% dimethylsulfoxide) for 3 h at room temperature. The samples were washed with PBSTw (1×PBS and 0.1% Tween-20), post-fixed with ethanol:acetic acid (2:1) at −20 °C for 20 min and washed with PBSTw. The embryos were blocked overnight at 4 °C with 5% BSA, washed with PBSTw, blocked with Avidin D solution (Vector Laboratories) for 30 min at room temperature, and washed with PBSTw. They were then blocked with Biotin solution (Vector Laboratories) for 30 min at room temperature, washed with PBSTw and incubated with equilibration buffer (1×TdT

reaction buffer, 1×$CoCl_2$ and 1×PBS; Roche) for 1 h at room temperature. The samples were incubated in TdT reaction mix (600 units of Terminal Transferase, Biotin-16 UTP, Equilibration Buffer; Roche) at 37 °C for 4 h and washed 6 × 15 min with PBSTw. Tg(*fli1:GFP*) embryos were incubated overnight with anti-GFP antibody (1:500; Aves Lab) at 4 °C. These were washed 6 X 15 min with PBSTw and incubated with anti-strepavidin-Alexa647 antibody (1:500; ThermoFisher), goat anti-chicken Alexa Flour 488 secondary antibody (1:500; ThermoFisher) and DAPI (1:1,000; Life Technologies) at room temperature for 3 h. The embryos were washed 6 × 15 min with PBSTw and mounted in Vectashield (Vector Laboratories).

### Detection of apoptotic cell death by acridine orange staining.

Dechorionated embryos were incubated in 50 μg $ml^{-1}$ acridine orange solution (Sigma) in E3 water for 1 h, protected from light. After three washes in 1×E3 water, the embryos were imaged by confocal microscopy.

### ChIP-seq.

Approximately 2,000 WT or mutant *supt16h* embryos were collected for two technical replicates and deyolked in Ginzburg fish Ringer solution. The embryos were resuspended in 1 ml PBS with 1 mM PMSF, 1×cOmplete EDTA-free protease inhibitor cocktail tablet (Roche) and 1×phosSTOP phosphatase inhibitor tablet (Roche), and pushed through a 21 G needle. The embryos were crosslinked with 4 mM DSG (ProteoChem) for 30 min, followed by 1% PFA for 8 min and stopped with 0.125 M glycine. The fixed embryos were resuspended in 1 ml Lysis buffer 1 (0.05 M HEPES, 140 mM NaCl, 1 mM EDTA, 1% glycerol, 0.5% NP40 and 0.25% Triton-X100) and lysed on the TissueRuptorII (Qiagen) for 20 s, low. The tissues were rocked for 10 min at 4 °C, pelleted and resuspended in 1 ml Lysis buffer 2 (10 mM Tris, pH 8, 200 mM NaCl, 1 mM EDTA and 0.5 mM EGTA). They were rocked again for 10 min at room temperature, pelleted and resuspended in 1.5 ml Lysis buffer 3 (10 mM Tris, pH 8, 100 mM NaCl, 1 mM EDTA, 0.5 mM EGTA, 0.1% sodium deoxycholate and 0.05% SDS). The tissues were sonicated using a Diagenode Bioruptor 300 (30 s on, 30 s off; high; 34 cycles). Triton-X100 (0.8%) was added and the cells were spun down. An aliquot of the lysate (20 μl) was saved to be used as an input control and the remainder was incubated overnight with Dynabeads bound with 10 μg p53 antibody (GeneTex) at 4 °C with rotation. The beads were collected on a magnet and washed 1× with Wash buffer 1 (20 mM Tris, pH 8, 150 mM NaCl, 2 mM EDTA, 0.1% SDS and 1% Triton-X100), 1× with Wash buffer 2 (20 mM Tris, pH 8, 500 mM NaCl, 2 mM EDTA, 0.1% SDS and 1% Triton-X100), 1× with Wash buffer 3 (10 mM Tris, pH 8, 250 mM LiCl, 1 mM EDTA, 1% sodium deoxycholate and 1% NP40), 3× with TET buffer (1×TE and 0.2% Tween-20) and 1× with TE-NaCl (1×TE and 50 mM NaCl). The beads were resuspended in 500 μl Elution buffer (50 mM $NaHCO_3$ and 1% SDS) and incubated overnight with 0.2 M NaCl at 65 °C. The lysate was incubated for 2 h at 37 °C with 5 μl RNase A (10 mg $ml^{-1}$) and 2 h at 55 °C with 5 μl proteinase K (20 mg $ml^{\mu 1}$). DNA was purified using phenol-chloroform-isoamyl alcohol and resuspended in 50 μl TE (10 mM Tris, pH 8 and 1 mM EDTA). A TruSeq ChIP library preparation kit (Illumina) was used to construct SR75 libraries run on an Illumina HiSeq4000.

ChIP-seq data underwent quality assessments using FastQC 0.11.2 and MultiQC 1.5, and subsequent trimming of Illumina adaptors using Trimmomatic. STAR was used for sequence alignment using GRCz10 (ref. [69]) and HOMER was used to call and analyse the peaks[67]. Differential gene expression was analysed using DESeq2 1.18.1. The peaks were visualized using Integrative Genomics Viewer (IGV) 2.3.65 (ref. [68]).

### p53 Transactivation luciferase assay.

HCT116 (ATCC CCL-247) cells knocked out for p53 were maintained at 37 °C in McCoy's 5a medium modified with 10% heat-inactivated FBS. The *Danio rerio phc1* intron was cloned into pGL4.23 (5′-GAGACGGATCCATAACCATACATCAGTGGAAAGC-3′ and 5′-GTCTCGTCGACTGCTAGGAATGCACCGATAA-3′) and the 20-bp responsive element was deleted by Gibson assembly (5′-GCGTCGCACTTGCGTGGGCAAGTGCACTATAATGGAGCTTTC-3′ and 5′-AAGCTCCATTATAGTGCACTTGCCCACGCAAGTGCGACGC-3′). The HCT116 cells were transiently transfected with pGL4.23 constructs by X-tremeGENE HP DNA transfection reagent (Roche). The cells were harvested after 48 h and the luciferase activity was measured using a Dual-luciferase reporter assay system (Promega) and SYNERGY Neo2 multi-mode reader (BioTek).

### Statistics and reproducibility.

In all figures: NS, not significant ($P > 0.05$); *$P < 0.05$; **$P < 0.01$; ***$P < 0.001$ and ****$P < 0.0001$. Data were analysed using Prism 6 and 7 (GraphPad). A two-tailed Student's *t*-test was conducted to compare two sample groups. To test for significance in larger groups, one-way or two-way ANOVAs, corrected for multiple comparisons using Tukey's or Sidak's statistical hypothesis testing, respectively, were used. In addition, comparisons for multiple *t*-tests were corrected for using the Holm-Sidak method. All tests used a confidence interval of 0.05. *P* values less than 0.05 were considered significant. Sample sizes were chosen based on the number of independent experiments required for statistical significance and technical feasibility. The statistical methods used for comparisons are indicated in the relevant figure legends.

### Reporting Summary.

Further information on research design is available in the Nature Research Reporting Summary linked to this article.

## Data availability

Raw and processed RNA-seq (linkage mapping), RNA-seq (differential expression), ATAC-seq and ChIP-seq data have been deposited into the public functional genomics data repository Gene Expression Omnibus. The accession numbers for these data are GSE106342, GSE127555, GSE106341and GSE116088for RNA-seq (linkage mapping), RNA-seq (differential expression), ATAC-seq and ChIP-seq, respectively. All other data supporting the findings of this study are available from the corresponding author on reasonable request. Source data are provided with this paper.

## Extended Data

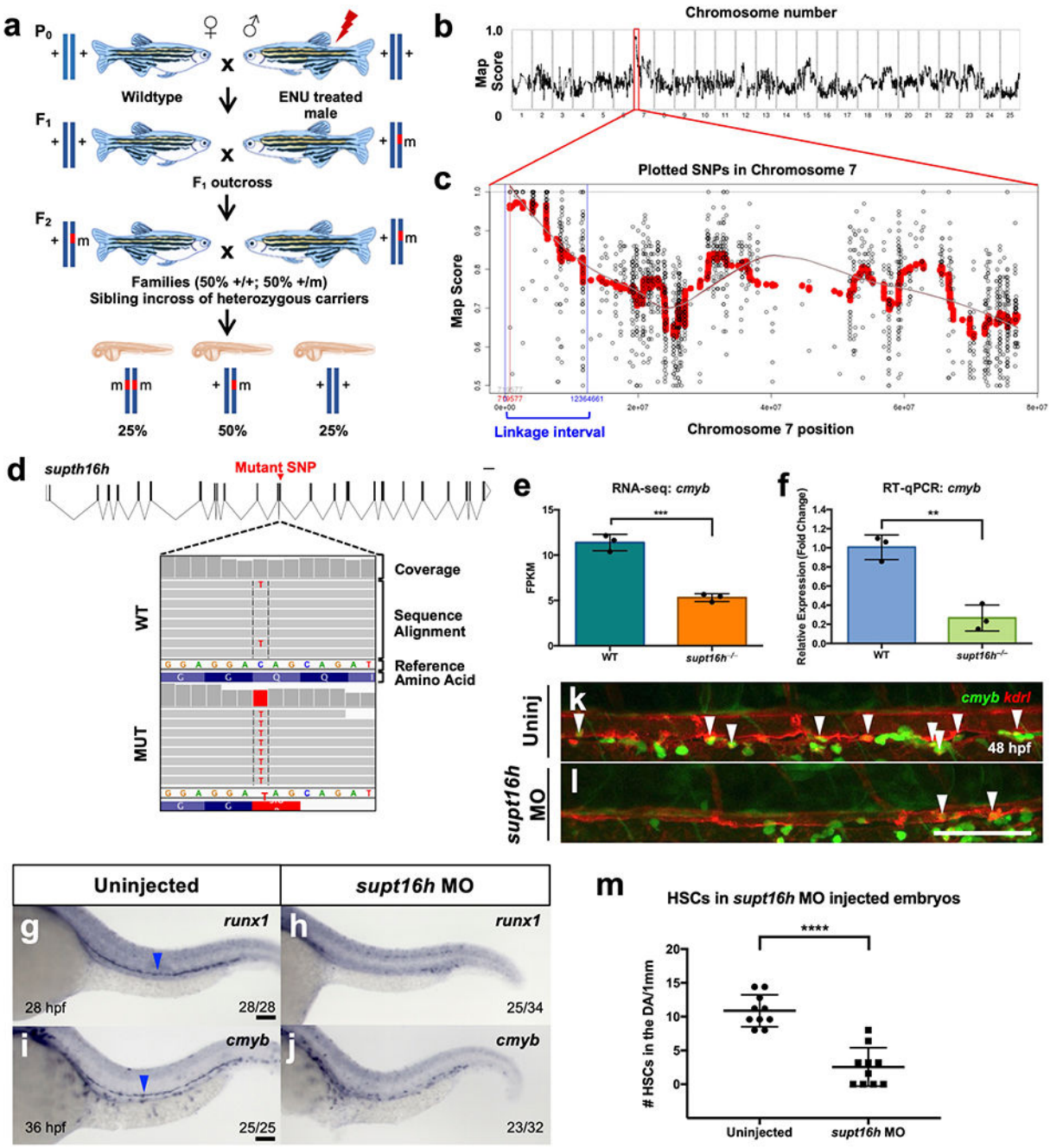


**Extended Data Fig. 1 |. Characterizing the causal mutation from our forward genetic screen.**
**a**, Diagram of the forward genetic screen strategy. **b,c**, Mapping of RNA-seq using RNAmapper with whole genome view (**b**) and specifically looking at the linked interval on Chr 7 (**c**). **d**, Position and RNA-seq coverage of SNP on *supt16h* resulting in a premature stop codon. **e,f**, Expression of *supt16h*$^{-/-}$ based on RNA-seq (**e**) (Represented as mean ± s.d., two-tailed Student's *t*-test, $n = 3$, $P = 0.0005$) and RT-qPCR (**f**) (Represented as mean ±

s.d., two-tailed Student's *t*-test, $n = 3$, $P = 0.0024$) for *cmyb.* For RT-qPCR, expressions are relative to WT sibling. **g-j**, WISH of WT embryos injected with *supt16h*-MO for *runx1* (blue arrowheads) at 28 hpf and *cmyb* at 36 hpf. **k,l**, Representative confocal of Tg(*cmyb:GFP;kdrl:mCherry*) embryos injected with *supt16h*-MO from one independent experiment. Double positive HSPCs indicated by white arrowheads at 48 hpf. DA = dorsal aorta; V = vein. **m**, Quantification of double positive HSPCs from (**g** and **h**) (Represented as mean ± s.e.m., two-tailed *t*-test, $n = 10$, $P < 0.0001$). Bar, 100 μm. Source data provided in Supplementary Table 5.

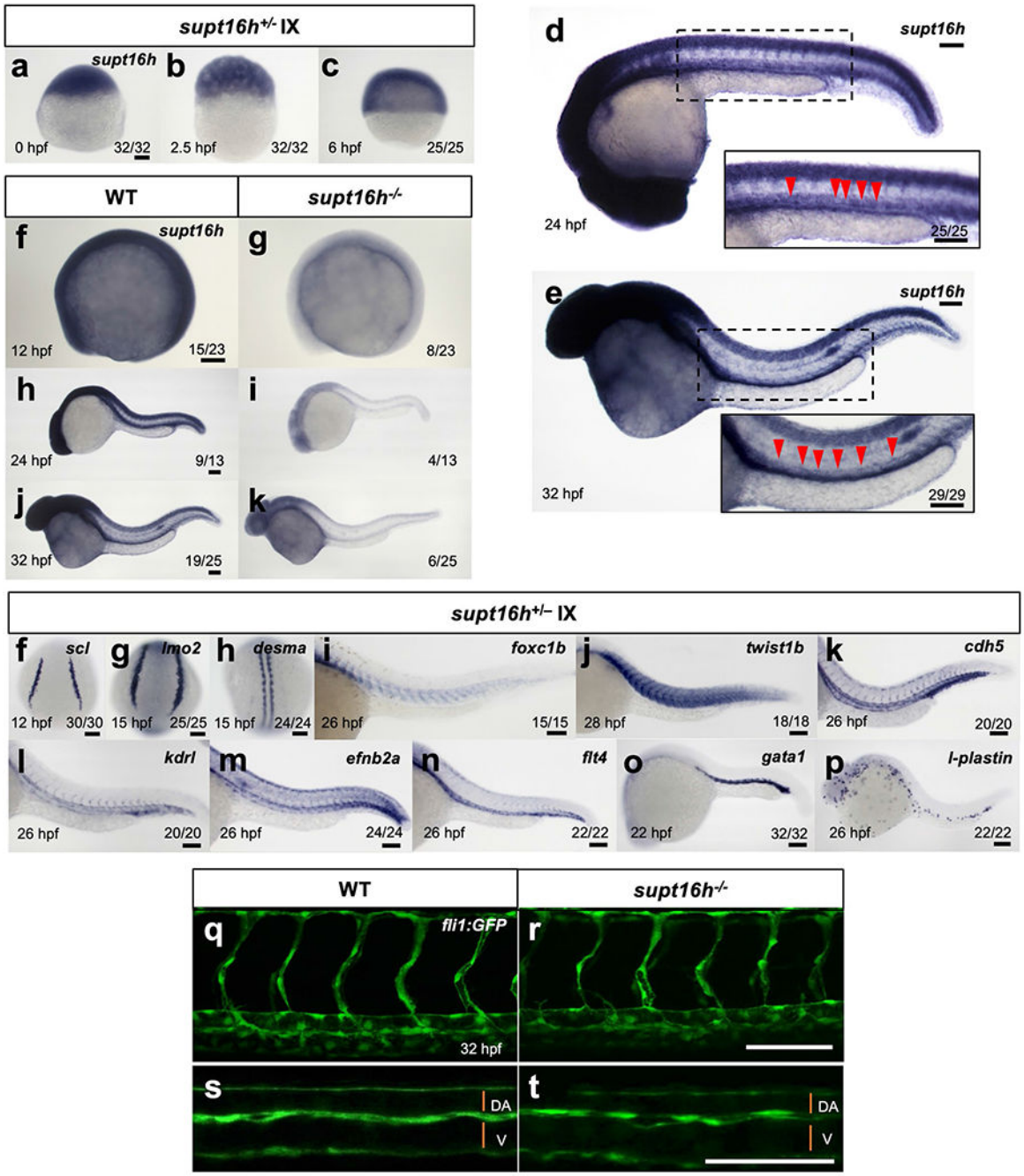


**Extended Data Fig. 2 |. The expression pattern of *supt16h* and the effect of its knockout on HSPC relevant tissues.**

**a-c**, WISH of embryos from a *supt16h*$^{+/-}$ incross (IX) for *supt16h* expression at 0, 2.5, and 6 hpf. **d,e**, WISH of WT embryos for *supt16h* expression at 24 and 32 hpf. Insets zoom magnify the DA (red arrowheads). **f-k**, WISH of WT sibling and *supt16h*$^{-/-}$ embryos for *supt16h* expression at 12, 24, and 32 hpf. **f-p**, WISH of *supt16h*$^{+/-}$ incross (IX) using probes for posterior lateral mesoderm (PLM) makers *scl*, and *lmo2* (**f,g**), somitic marker *desma* (**h**), sclerotome marker *foxc1b* and *twist1b* (**i,j**), endothelial markers *cdh5* and *kdrl* (**k,l**), arterial

marker *efnb2a* (**m**), venous marker *flt4* (**n**), primitive erythroid marker *gata1* (**o**), and primitive leukocyte marker *l-plastin* (**p**). **q,r**, Representative confocal of *supt16h*$^{-/-}$ and WT sibling embryos on *Tg(fli1:GFP)* background examining vasculature development. Based on one independent experiment. **s,t**, Magnified images of (**q,r**) highlight vein (V) and dorsal aorta (DA) formation. Bar, 100 μm.

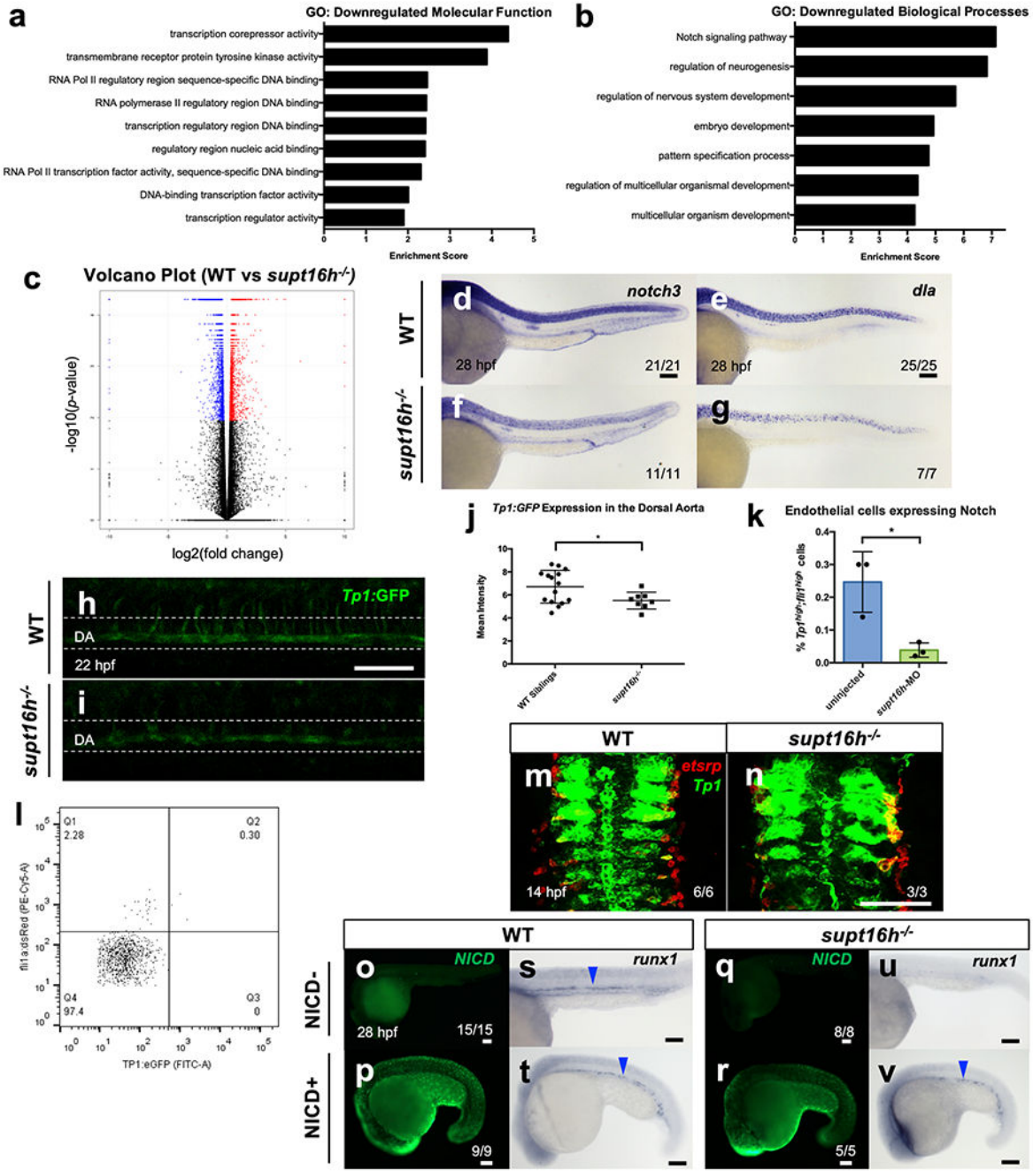


**Extended Data Fig. 3 |. Characterizing the effect of *supt16h* on Notch gene expression.**

**a,b**, Gene Ontology Analysis of Biological Components (**a**) and Molecular Components (**b**) shows downregulated genes in *supt16h*$^{-/-}$ embryos based on a log2fold change >1. **c**, Volcano plot of the differentially expressed genes between WT sibling and *supt16h*$^{-/-}$ embryos based on RNA-seq. Data representative of 3 (**a-c**) biological replicates. **d-g**, WISH of *supt16h*$^{-/-}$ and WT sibling embryos using probes for *notch3* and *dla.* **h,i** Representative confocal images along the DA of *supt16h*$^{-/-}$ and WT sibling embryos on *Tg(Tp1:GFP)* background at 22 hpf. Bar, 50 μm. **j**, Mean fluorescence level from (**h,i**) of *Tp1:GFP* along the DA calculated in ImageJ (Represented as mean ± s.e.m., two-tailed Student's *t*-test, $n_{WT}$= 15,$n_{MUT}$=8,$P$ = 0.0373). **k**, Sorted double positive *Tp1:GFP+;fli1:DsRed*$^{+}$ cells from *supt16h* morphants and uninjected controls at 22 hpf by flow cytometry (Represented as mean ± s.d, two-tailed Studentt's *t*-test, $n$ = 3,$P$ = 0.0192). **l**, Gating strategy used to quantify TP1 (Notch- FITC) + endothelial (PE-Cy5) cells. **m,n**, DFISH of *Notch-active* (green) and *etsrp* (red) tissues in *supt16h*$^{-/-}$ and WT sibling embryos on a *Tg(Tp1:GFP)* background at 14 hpf. Based on one independent experiment. **o-v**, Global expression of NICD$^{+}$ and NICD$^{-}$ embryos that are WT siblings or *supt16h*$^{-/-}$ *(supt16h*$^{+/-}$*;hsp70:gal4* x *supt16*$^{+/-}$*;UAS-myc:NICD)* analysed at 28 hpf by NICD immunohistochemistry (IHC) (**l-o**) and *runx1* WISH (**p-s**). Representative images from two independent experiments. Bar, 100 μm. Blue arrowheads indicate HSPCs. Bar, 100 μm. Source data provided in Supplementary Table 5.

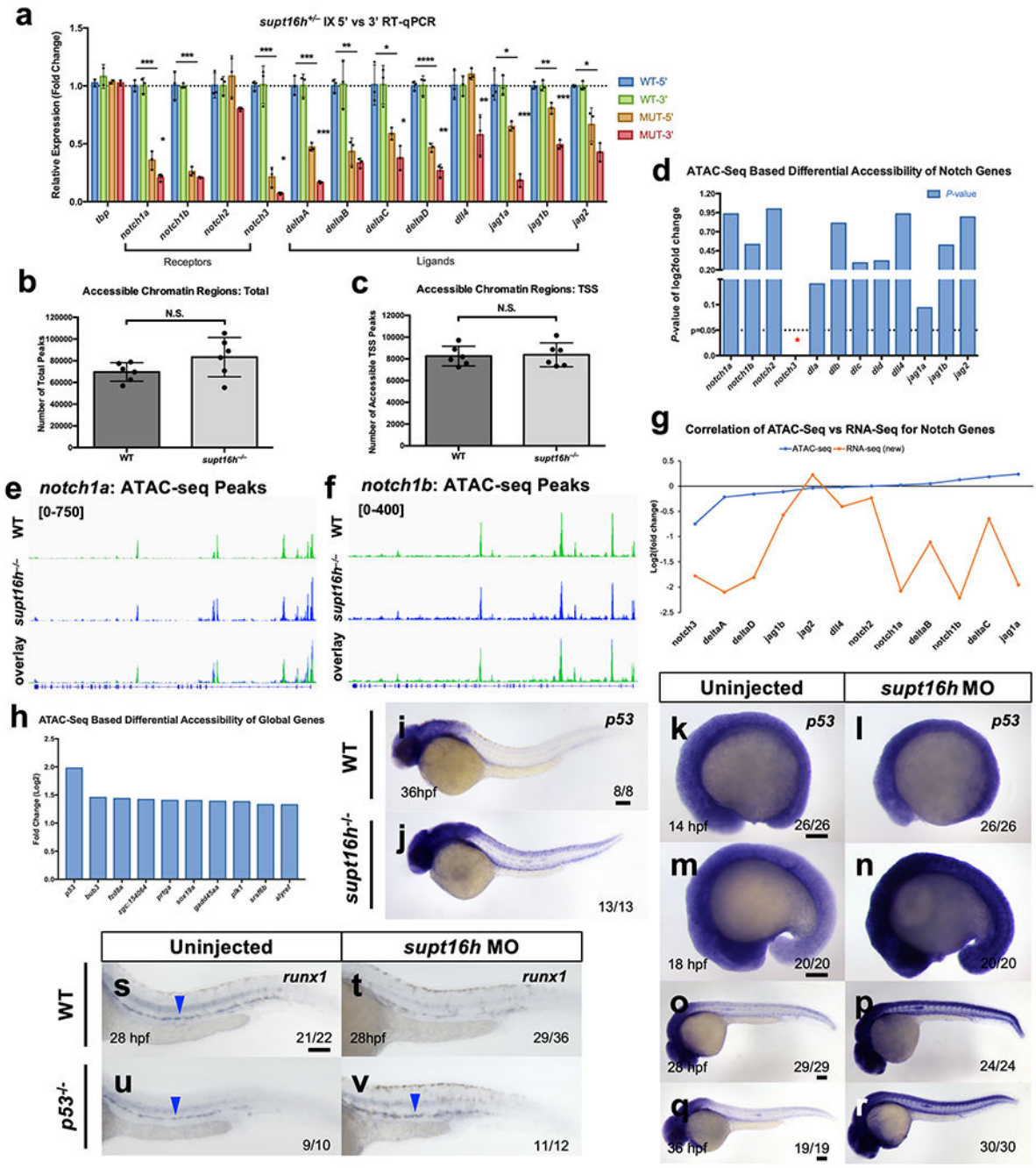


**Extended Data Fig. 4 |. The effect of *supt16h* on transcript elongation and chromatin accessibility.**

**a**, RT-qPCR of 5′ vs 3′ initiation/elongation of Notch genes in WT sibling and *supt16h*$^{-/-}$ embryos at 32 hpf. Expressions relative to WT sibling (horizontal dotted line) (Represented as mean ± s.d, two-tailed Student's *t*-test with Holm-Sidak correction for multiple comparisons, $n = 3$, ***$P < 0.001$, **$P < 0.01$, *$P < 0.05$ lined significance compares WT 5′ to MUT 3′, significance over MUT 5′ compares MUT 5′ to MUT 3′). **b**, ATAC-seq results plotting the total number of accessible peaks in WT and *supt16h*$^{-/-}$ embryos at 32 hpf

(Represented as mean ± s.d, two-tailed *t*-test, $n = 6$, N.S. = not significant). **c**, ATAC-seq results plotting the number of accessible TSS peaks in WT sibling and *supt16h*$^{-/-}$ embryos (Represented as mean ± s.d, two-tailed Student's *t*-test, $n = 6$, N.S. = not significant). **d**, *p*-values of the differential accessibility of Notch genes based on ATAC-seq log2fold change of *supt16h*$^{-/-}$ vs WT sibling. **e,f**, ATAC-seq peak plot of chromatin accessibility in *supt16h*$^{-/-}$ and WT sibling embryos for *notch1a* and *notch1b*. Bottom panel shows peak overlay. **g**, Plot of ATAC-seq log2fold change by increasing accessibility vs. corresponding RNA-seq log2fold change values. **h**, Rank order of top 10 differentially accessible genes based on ATAC-seq of *supt16h*$^{-/-}$ and WT sibling embryos at 32 hpf. **i,j**, WISH of *p53* in WT sibling and *supt16h*$^{-/-}$ embryos at 36 hpf. **k-r**, WISH of *p53* in embryos injected with *supt16h*-MO at 14, 18, 28, and 36 hpf. **s-v**, WISH of *runx1* (blue arrowheads) for WT sibling and *p53*$^{y-}$ injected with *supt16h*-MO. Data representative of 2 (**i-r**) and 3 (**a,h**) biological replicates. Bar, 100 μm. Source data provided in Supplementary Table 5.

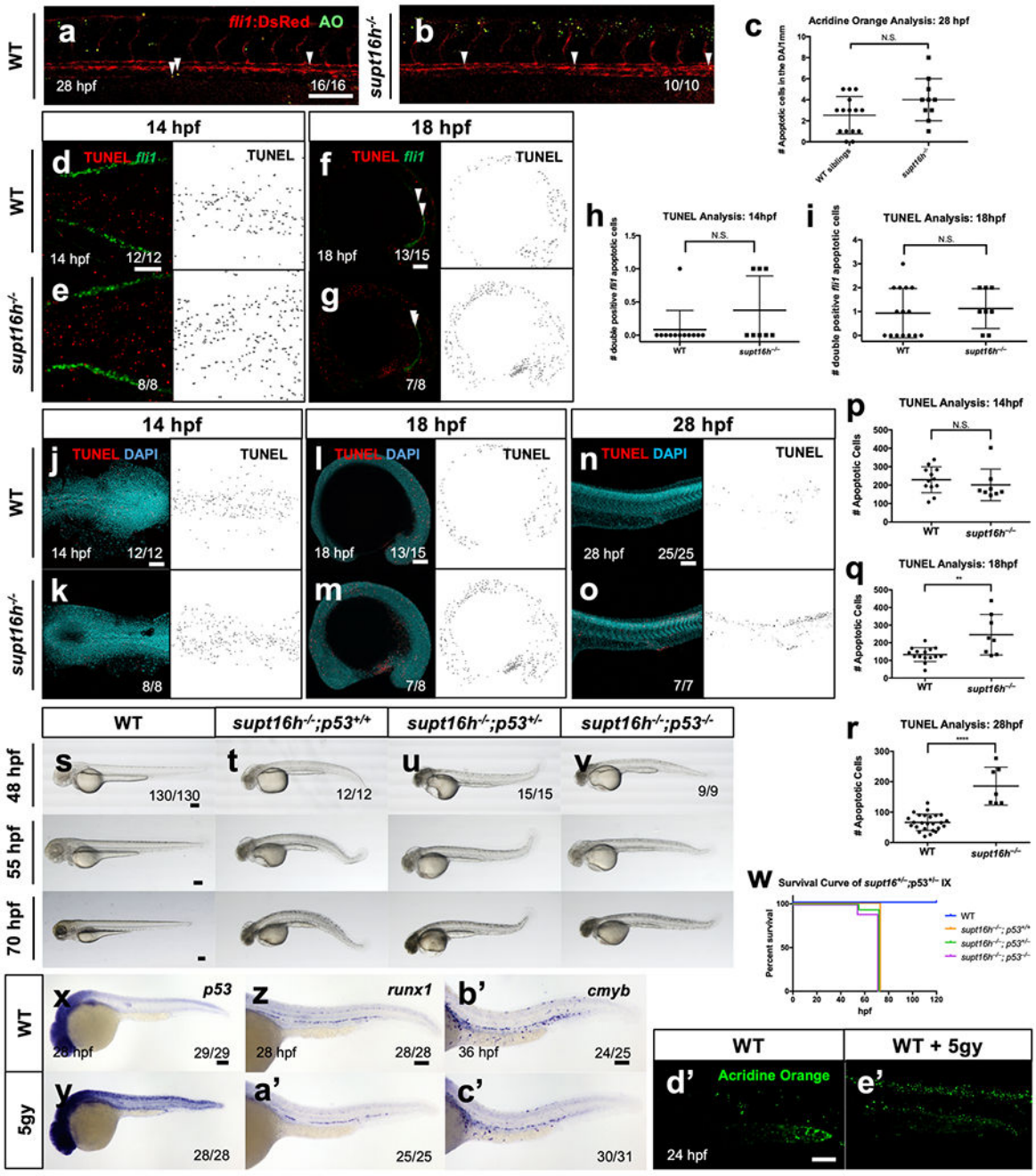


**Extended Data Fig. 5 |. Characterizing P53-mediated apoptosis in *supt16h*$^{-/-}$ embryos.**

**a,b**, Representative confocal of WT sibling and *supt16h*$^{-/-}$*;Tg(fli1.GFP)* and stained with Acridine Orange (AO) at 28 hpf. (arrowheads = TUNEL$^{+}$;*fli1*$^{+}$ cells). **c**, Quantification of double positive TUNEL+;*fli1*+ cells for (**a,b**) ($n_{WT}$ = 15, $n_{MUT}$ = 10, N.S. = not significant). **d-g**, TUNEL of WT sibling and *supt16h*$^{-/-}$ crossed onto *Tg(fli1.GFP)* at 14 and 18 hpf (arrowheads = TUNEL$^{+}$;*fli1*$^{+}$ cells). Confocal images of TUNEL, *fli1* and double-positive TUNEL$^{+}$*fli1*$^{+}$ (yellow; indicated by white arrowheads; left), and TUNEL-only cells are shown (right). **h,i**, Quantification of double positive TUNEL+;*fli1*+ cells for 14 (**h**) ($n_{WT}$ =

12, $n_{MUT}$= 8, N.S. = not significant) and 18 hpf (**i**) (*nWT* = 12, *nMUT* = 8, N.S. = not significant). **j-o**, TUNEL of WT sibling and *supt16h*$^{-/-}$ at 14 hpf, 18 hpf, and 28 hpf. Confocal images of TUNEL and DAPI (left) and TUNEL-only cells are shown (right). **p-r**, Quantification of apoptotic cells based on TUNEL at 14 hpf ($n_{WT}$ = 12, $n_{MUT}$ = 8, N.S. = not significant), 18 hpf ($n_{WT}$ = 15, $n_{MUT}$ = 8, ***P* = 0.0023), and 28 hpf ($n_{WT}$ = 25, $n_{MUT}$ = 7, *****P* < 0.0001). **s-v**, Brightfield images of WT sibling or *supt16h*$^{-/-}$ in the context of *p53* WT ($^{+/+}$); HET($^{+/-}$); MUT($^{-/-}$) embryos at 48, 55, and 70 hpf. **w**, Kaplan-Meier survival curve for (**s-v**). **x-c′**, WISH of *p53, runx1*, and *cmyb* for WT embryos treated with 5 gy of ionizing radiation at 6 hpf. d′,e′, AO staining at 24 hpf following treatment of WT embryos with 5 gy of ionizing radiation at 6 hpf. Representative images based on one independent experiment. Dot plot graphs (**c**, **h**, **i**, **p**, **q**, **r**) represented as mean ± s.d., two-tailed Student's *t*-test. Bar, 100 μm. Source data provided in Supplementary Table 5.

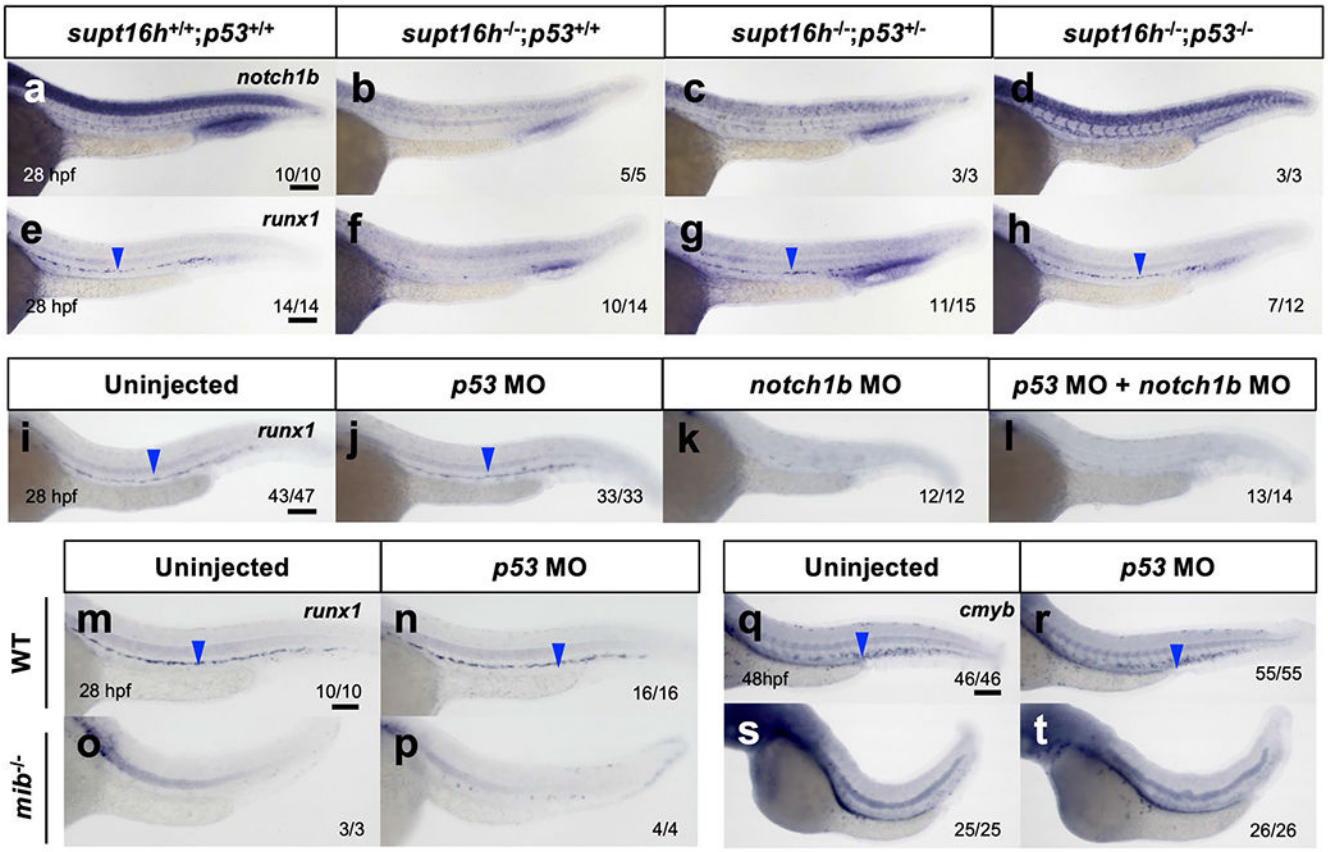


**Extended Data Fig. 6 |. Characterizing the effect of *p53* on Notch gene expression and HSPC formation.**

**a-h**, WISH of WT sibling **(a,e)** and *supt16h*$^{-/-}$ embryos that are *p53*$^{+/+}$ (**b,f**), *p53*$^{+/-}$ **(c,g)**, or *p53*$^{-/-}$ **(d,h)** for *notch1b* **(a-d)** and *runx1* **(e-h)** at 28 hpf. **i-l**, WISH for *runx1* of embryos injected with *p53*-MO, *notch1b*-MO, or both MOs at 28 hpf. **m-t**, WISH of *runx1* **(m-p)** and *cmyb* **(q-t)** for WT sibling or *mib* $^{-/-}$ embryos injected with *p53*-MO. Blue arrowheads indicate HSPCs. Bar, 100 μm.

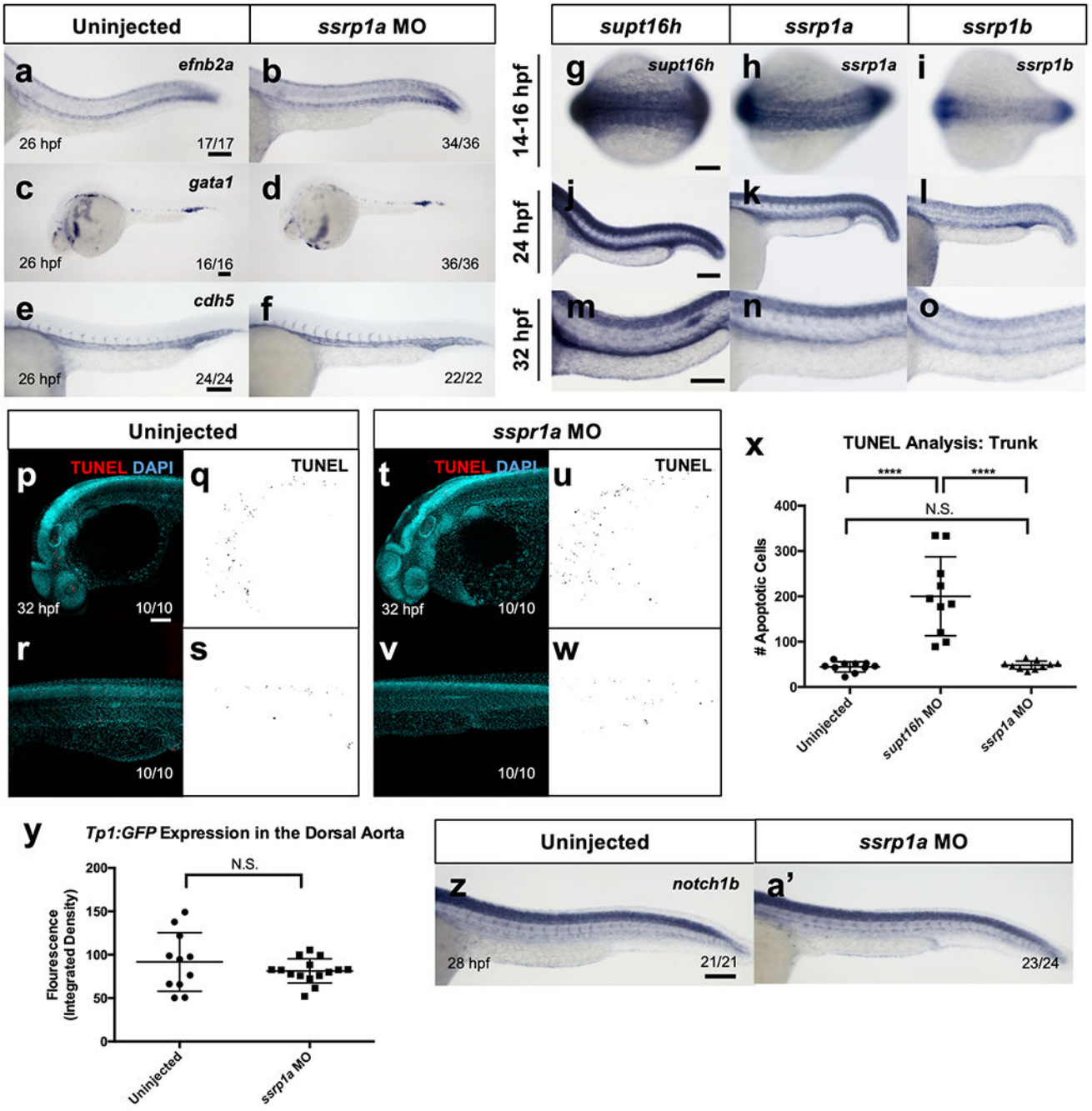


**Extended Data Fig. 7 |. Characterizing the expression profile and effect of *ssrp1a*on HSPCs.**
**a-f**, WISH of embryos injected with *ssrp1a*-MO and probed with *efnb2a* (**a,b**), *gata1* (**c,d**), and *cdh5* (**e,f**) at 26 hpf. No effect is seen on dorsal aorta, red blood cell, or vasculature formation upon *ssrp1a* knockdown. **g-o**, WISH of *supt16h, ssrp1a*, and *ssrp1b* for WT embryos at 14–16 hpf with a dorsal view (**g-i**), and 24 hpf (**j-l**) and 32 hpf with a posterior lateral view (**m-o**). **p-w**, TUNEL of uninjected (**p-s**) and *ssrp1a*-MO (**t-w**) embryos at 32 hpf. Confocal images of TUNEL and DAPI (left) and TUNEL only (right) are shown. **x**, Quantification of the number of apoptotic cells in *ssrp1a* morphants from (**p-w**) based on

TUNEL for the trunk region (Represented as mean ± s.d., one-way ANOVA with post-hoc Tukey, $n = 10$, $P < 0.0001$, N.S. = not significant). **y**, Mean fluorescence level of *Tp1:GFP* of the DA calculated in ImageJ based on Integrated Density (Represented as mean ± s.d., two-tailed *t*-test, $n_{WT} = 11$, $n_{MO} = 15$, $^{*}P = 0.0147$, N.S. = not significant). **z,a'**, WISH of *notch1b* in WT sibling and *ssrp1a*$^{-/-}$ embryos at 28 hpf. Data representative of 2 (**g-o**) biological replicates. Bar, 100 μm. Source data provided in Supplementary Table 5.

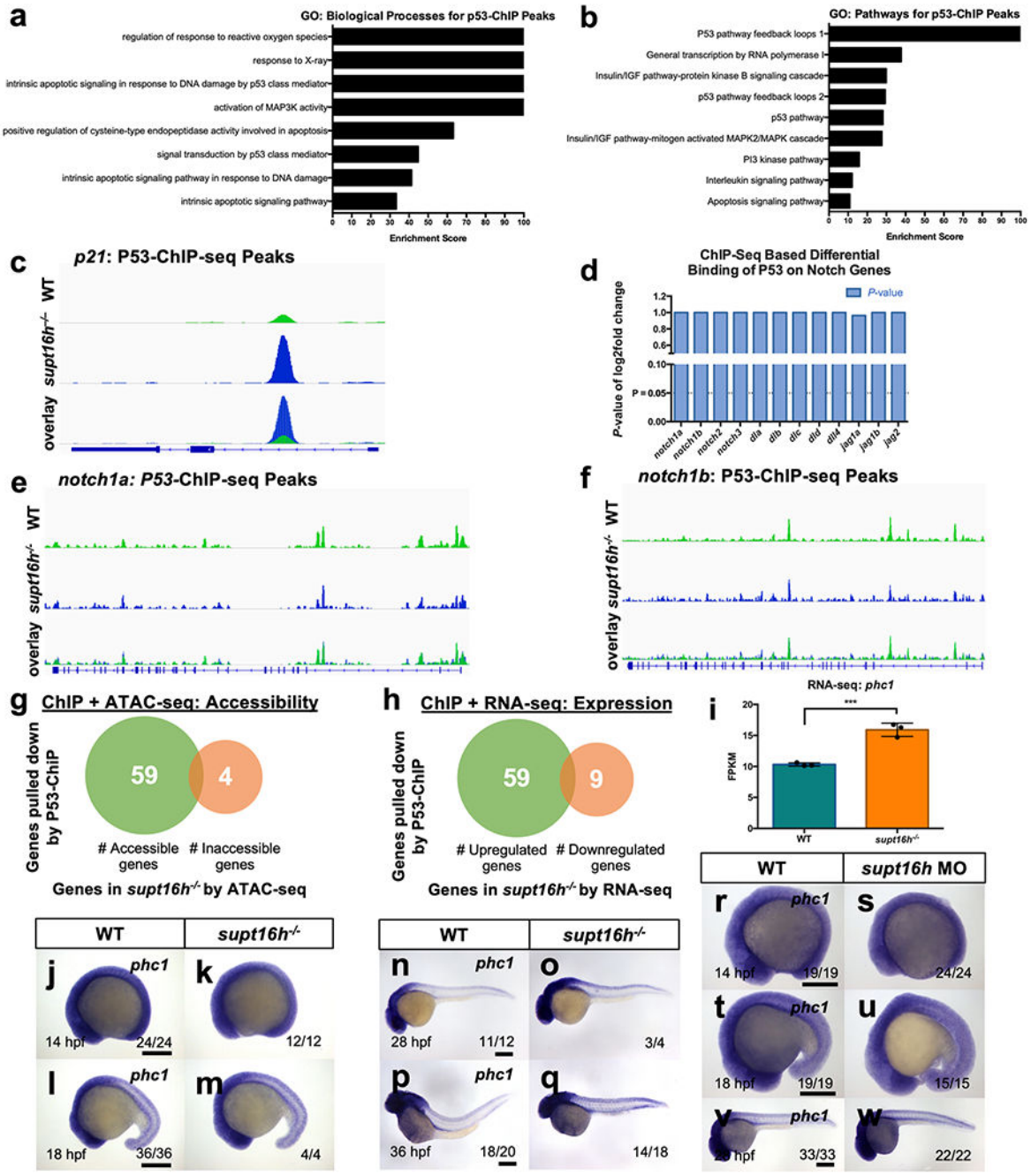


**Extended Data Fig. 8 |. Characterizing the role of P53 on modulating Notch expression.**

**a,b**, Gene Ontology analysis of the significant p53-ChIP-peaks for the Biological Processes and Pathways affected. **c**, Plot of p53-ChIP-seq peaks for a known p53-target gene, *p21.* **d**, Graph of *P*-values representing the log2 fold change of the differential binding of p53 to Notch genes between WT sibling and *supt16h*$^{-/-}$ embryos. No significant effect is observed in biding to Notch genes. **e,f**, p53-ChIP-seq plots for *notch1a* and *notch1b*, graphing WT sibling and *supt16h*$^{-/-}$ peaks. **g**, Venn diagram depicting the number of accessible (green) and inaccessible (orange) p53-bound genes based on p53-ChIP-seq and ATAC-seq of WT sibling and *supt16h*$^{-/-}$ embryos at 32 hpf. Genes possessing significant p53-bound peaks ($n$ = 2 for ChIP-seq, $n$ = 6 for ATAC-seq, two-tailed Student's $t$-test, adjusted $P > 0.05$) were assessed for their accessibility based on ATAC-seq (two-tailed t-test, adjusted $P > 0.05$), where genes had at least >1 Log2 fold change between WT and *supt16h*$^{-/-}$ samples. **h**, The number of upregulated (green) and downregulated (orange) p53-bound genes based on p53-ChIP-seq and RNA-seq of WT sibling and *supt16h*$^{-/-}$ embryos at 32 hpf. Genes possessing significant p53-bound peaks ($n$ = 2 for ChIP-seq, $n$ = 3 for RNA-seq, two-tailed Student's $t$-test, adjusted $P > 0.05$), where genes had at least >1 Log2 fold change between WT and *supt16h*$^{-/-}$ samples, were assessed for their expression based on RNA-seq (two-tailed $t$-test, adjusted $P > 0.05$). p53 binding stimulates increased gene expression. **i**, Expression of *phc1* in *supt16h* mutants and WT siblings based on RNA-seq (Represented as mean ± s.d, two-tailed Student's $t$-test, $n$= 3, $P$= 0.0009). **j-q**, WISH of *phc1* expression in WT sibling and *supt16h*$^{-/-}$ embryos at 14 (**j,k**), 18 (**l,m**), 28 (**n,o**), and 36 hpf (**p,q**). r-w, WISH of *phc1* expression in uninjected and *supt16h*-MO injected embryos at 14 (**r,s**), 18 (**t,u**), and 28 (**v,w**). Bar, 200 μm. Source data provided in Supplementary Table 5.

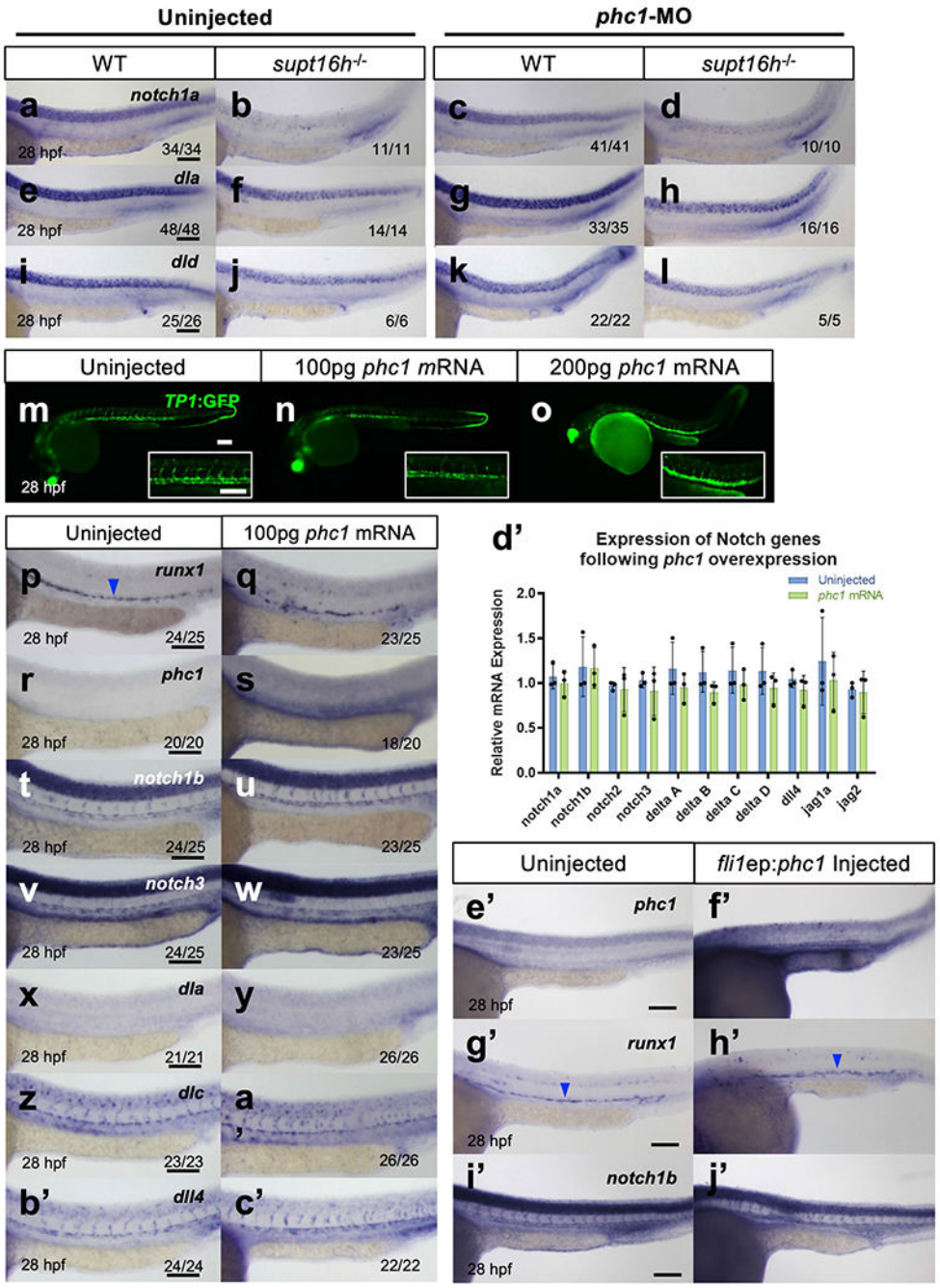


**Extended Data Fig. 9 |. Characterizing the effect of *phc1* overexpression on Notch signalling.** **a-l**, WISH of WT sibling and *supt16h*$^{-/-}$ embryos injected with *phc1*-MO probed for *notch1a, dla*, and *dlc* at 28 hpf. **m-o**, Representative confocal images of wild-type embryos on a *Tg(Tp1:GFP)* background injected with 100 and 200 pg of *phc1* mRNA at 28 hpf. Insets are magnified images of the DA and intersomitic vessels. Representative images from one independent experiment. **p-c′**, WISH of wild-type embryos injected with 100 pg of *phc1* mRNA probed for at 28 hp for *runx1* (**p-q**), *phc1* (**r-s**), *notch1b* (**t-u**), *notch3* (**v-w**), *dla* (x-y), *dlc* (z-a′), and *dll4* (**b-c′**). **d′**, RT-qPCR of Notch genes in WT sibling and embryos

injected with 100 pg (r) of *phc1* mRNA collected at 28 hpf. No significant changes observed between samples. (Represented as mean ± s.d., two-tailed Student's t-test with Holm-Sidak correction for multiple comparisons, $n = 3$). **e′-j′**, WISH at 28 hpf for *phc1* (**e′-f′**), *runx1* (**g′-h′**), and *notch1b* (**i′-j′**) of wild-type embryos injected with *fli1ep:phc1* plasmid for transient expression of *phc1* in the vasculature. Blue arrowheads indicate HSPCs. Bar, 100 μm.

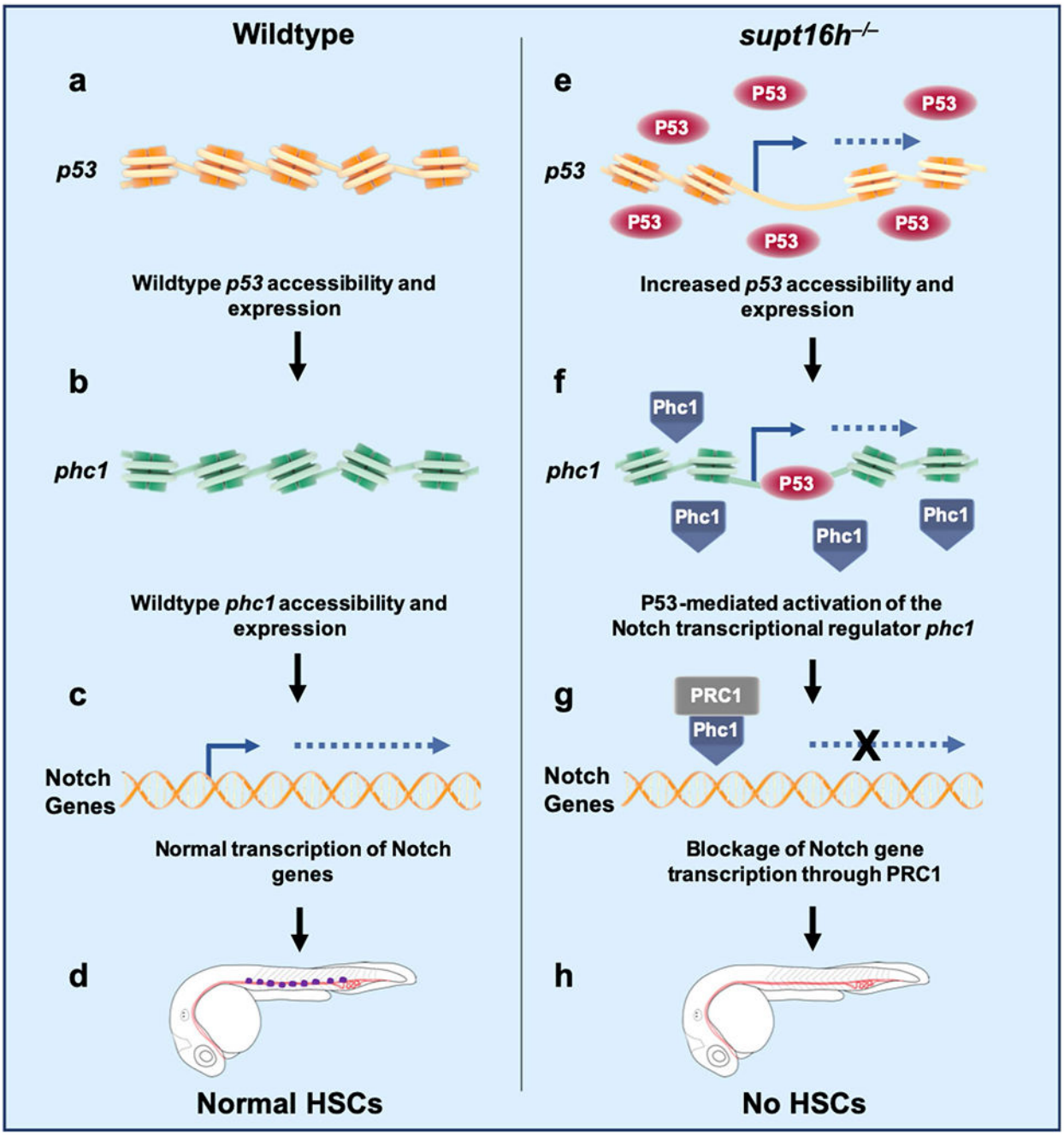


**Extended Data Fig. 10 |. Model of how Supt16h and P53 regulate HSPC specification through notch transcription.**

**a,b,** In a wild-type settng, *p53* **(a)** and *phc1* (b) maintain baseline levels of accessibility and transcriptional expression. **c,d,** This results in normal transcription of Notch genes **(c)** and allows for proper specification of HSPCs **(d). e,** In *supt16h* mutants, the *p53* gene locus is highly accessible, resulting in increased *p53* mRNA and protein levels. **f**, p53 then binds to *phc1*, a repressor of Notch gene expression, to allow for its enhanced expression. **g**, PHC1, as part of PRC1, inhibits Notch signalling by acting as direct or indirect a transcriptional repressor of Notch genes. **h**, In the absence of Notch expression, HSPCs fail to specify.

## Supplementary Material

Refer to Web version on PubMed Central for supplementary material.

## Acknowledgements

This work was supported by the National Science Foundation Graduate Research Fellowship Program (grant no. DGE-1650112), UCSD Genetics Training Grant (grant no. T32GM008666-17), National Institutes of Health (grant no. R01-DK074482) and Institute for Basic Science (grant no. IBS-R022-D1). RNA-seq, ATAC-seq and ChIP-seq were conducted at the IGM Genomics Center, University of California, San Diego (MCC grant no. P30CA023100). We thank K. Ong, Y. G. Han, J. Park and S.-W. Jin for their technical assistance, J. Posakony for scientific guidance and the members of the D.T. laboratory for providing helpful comments.

## References

1. Ciau-Uitz A, Monteiro R, Kirmizitas A & Patient R Developmental hematopoiesis: ontogeny, genetic programming and conservation. Exp. Hematol 42, 669–683 (2014). [PubMed: 24950425]
2. Bertrand JY et al. Haematopoietic stem cells derive directly from aortic endothelium during development. Nature 464, 108–111 (2010). [PubMed: 20154733]
3. Espín-Palazón R et al. Proinflammatory signaling regulates hematopoietic stem cell emergence. Cell 159, 1070–1085 (2014). [PubMed: 25416946]
4. Hondele M et al. Structural basis of histone H2A-H2B recognition by the essential chaperone FACT. Nature 499, 111–114 (2013). [PubMed: 23698368]
5. Saunders A et al. Tracking FACT and the RNA polymerase II elongation complex through chromatin in vivo. Science 301, 1094–1096 (2003). [PubMed: 12934007]
6. Hsieh F-K et al. Histone chaperone FACT action during transcription through chromatin by RNA polymerase II. Proc. Natl Acad. Sci. USA 110, 7654–7659 (2013). [PubMed: 23610384]
7. Kumano K et al. Notch1 but not Notch2 is essential for generating hematopoietic stem cells from endothelial cells. Immunity 18, 699–711 (2003). [PubMed: 12753746]
8. Kim AD et al. Discrete Notch signaling requirements in the specification of hematopoietic stem cells. EMBO J. 33, 2363–2373 (2014). [PubMed: 25230933]
9. Clements WK et al. A somitic Wnt16/Notch pathway specifies haematopoietic stem cells. Nature 474, 220–224 (2011). [PubMed: 21654806]
10. Robert-Moreno À et al. Impaired embryonic haematopoiesis yet normal arterial development in the absence of the Notch ligand Jagged1. EMBO J. 27, 1886–1895 (2008). [PubMed: 18528438]
11. Vousden KH & Lane DP p53 in health and disease. Nat. Rev. Mol. Cell Biol 8, 275–283 (2007). [PubMed: 17380161]
12. Levine AJ & Berger SL The interplay between epigenetic changes and the p53 protein in stem cells. Genes Dev. 31, 1195–1201 (2017). [PubMed: 28765161]
13. Beckerman R & Prives C Transcriptional regulation by p53. Cold Spring Harb. Perspect. Biol 2, a000935 (2010). [PubMed: 20679336]
14. Miller AC, Obholzer ND, Shah AN, Megason SG & Moens CB RNA-seq-based mapping and candidate identification of mutations from forward genetic screens. Genome Res. 23, 679–686 (2013). [PubMed: 23299976]

15. Ashburner M et al. Gene Ontology: tool for the unification of biology. Nat. Genet 25, 25–29 (2000). [PubMed: 10802651]
16. Thomas PD Expansion of the gene ontology knowledgebase and resources: the Gene Ontology consortium. Nucleic Acids Res. 45, D331–D338 (2017). [PubMed: 27899567]
17. Burns CE, Traver D, Mayhall E, Shepard JL & Zon LI Hematopoietic stem cell fate is established by the Notch–Runx pathway. Genes Dev. 19, 2331–2342 (2005). [PubMed: 16166372]
18. Grainger S et al. Wnt9a is required for the aortic amplification of nascent hematopoietic stem cells. Cell Rep. 17, 1595–1606 (2016). [PubMed: 27806298]
19. Sturgeon CM, Ditadi A, Awong G, Kennedy M & Keller G Wnt signaling controls the specification of definitive and primitive hematopoiesis from human pluripotent stem cells. Nat. Biotechnol 32, 554–561 (2014). [PubMed: 24837661]
20. Ruiz-Herguido C et al. Hematopoietic stem cell development requires transient Wnt/β-catenin activity. J. Exp. Med 209, 1457–1468 (2012). [PubMed: 22802352]
21. Kobayashi I et al. Jam1a–Jam2a interactions regulate haematopoietic stem cell fate through Notch signalling. Nature 512, 319–323 (2014). [PubMed: 25119047]
22. Hadland BK et al. A requirement for Notch1 distinguishes 2 phases of definitive hematopoiesis during development. Blood 10.1182/blood-2004-03-1224 (2004).
23. Andersson ER, Sandberg R & Lendahl U Notch signaling: simplicity in design, versatility in function. Development 138, 3593–3612 (2011). [PubMed: 21828089]
24. Bai X et al. TIF1γ controls erythroid cell fate by regulating transcription elongation. Cell 142, 133–143 (2010). [PubMed: 20603019]
25. Berghmans S et al. *tp53* Mutant zebrafish develop malignant peripheral nerve sheath tumors. Proc. Natl. Acad. Sci. USA 10.1073/pnas.0406252102 (2005).
26. Ljungman M, Zhang F, Chen F, Rainbow AJ & McKay BC Inhibition of RNA polymerase II as a trigger for the p53 response. Oncogene 18, 583–592 (1999). [PubMed: 9989808]
27. Lindahl T & Wood RD Quality control by DNA repair. Science 286, 1897–1905 (1999). [PubMed: 10583946]
28. Itoh M et al. Mind bomb is a ubiquitin ligase that is essential for efficient activation of Notch signaling by Delta. Dev. Cell 4, 67–82 (2003). [PubMed: 12530964]
29. Orphanides G, LeRoy G, Chang CH, Luse DS & Reinberg D FACT, a factor that facilitates transcript elongation through nucleosomes. Cell 92, 105–116 (1998). [PubMed: 9489704]
30. Koltowska K et al. Ssrp1a controls organogenesis by promoting cell cycle progression and RNA synthesis. Development 140, 1912–1918 (2013). [PubMed: 23515471]
31. Huang H-T et al. A network of epigenetic regulators guides developmental haematopoiesis in vivo. Nat. Cell Biol 15, 1516–1525 (2013). [PubMed: 24240475]
32. Busch-Nentwich E et al. Sanger Institute Zebrafish Mutation Project mutant data submission. https://zfin.org/ZDB-ALT-160601-1382 (2013).
33. Smeenk L et al. Characterization of genome-wide p53-binding sites upon stress response. Nucleic Acids Res. 10.1093/nar/gkn232 (2008).
34. El-Deiry WS, Kern SE, Pietenpol JA, Kinzler KW & Vogelstein B Definition of a consensus binding site for p53. Nat. Genet 10.1038/ng0492-45 (1992).
35. Le Bouteiller M et al. Notchless-dependent ribosome synthesis is required for the maintenance of adult hematopoietic stem cells. J. Exp. Med 210, 2351–2369 (2013). [PubMed: 24062412]
36. Martinez A-M et al. Polyhomeotic has a tumor suppressor activity mediated by repression of Notch signaling. Nat. Genet 41, 1076–1082 (2009). [PubMed: 19749760]
37. Boyer LA et al. Polycomb complexes repress developmental regulators in murine embryonic stem cells. Nature 441, 349–353 (2006). [PubMed: 16625203]
38. Bracken AP, Dietrich N, Pasini D, Hansen KH & Helin K Genome-wide mapping of Polycomb target genes unravels their roles in cell fate transitions. Genes Dev. 20, 1123–1136 (2006). [PubMed: 16618801]
39. Lee TI et al. Control of developmental regulators by Polycomb in human embryonic stem cells. Cell 125, 301–313 (2006). [PubMed: 16630818]

40. Tolhuis B et al. Genome-wide profiling of PRC1 and PRC2 Polycomb chromatin binding in *Drosophila melanogaster*. Nat. Genet 10.1038/ng1792 (2006).
41. Ohta H et al. Polycomb group gene *rae28* is required for sustaining activity of hematopoietic stem cells. J. Exp. Med 195, 759–770 (2002). [PubMed: 11901201]
42. Ji YK et al. Defective long-term repopulating ability in hematopoietic stem cells lacking the Polycomb-group gene *rae28*. Eur. J. Haematol 73, 75–84 (2004). [PubMed: 15245505]
43. Keller DM et al. A DNA damage-induced p53 serine 392 kinase complex contains CK2, hSpt16, and SSRP1. Mol. Cell 7, 283–292 (2001). [PubMed: 11239457]
44. Keller DM & Lu H p53 serine 392 phosphorylation increases after UV through induction of the assembly of the CK2·hSPT16·SSRP1 complex. J. Biol. Chem 277, 50206–50213 (2002). [PubMed: 12393879]
45. Gasparian AV et al. Curaxins: anticancer compounds that simultaneously suppress NF-κB and activate p53 by targeting FACT. Sci. Transl. Med 3, 95ra74 (2011).
46. Kolundzic E et al. FACT sets a barrier for cell fate reprogramming in *Caenorhabditis elegans* and human cells. Dev. Cell 10.1016/j.devcel.2018.07.006 (2018).
47. Rhoades AR & Ruone FT Structural features of nucleosomes reorganized by yeast FACT and its HMG box component, Nhp6. Mol. Cell. Biol 24, 3907–3917 (2004). [PubMed: 15082784]
48. Westerfield M The Zebrafish Book. A Guide for the Laboratory Use of Zebrafish (Danio rerio) 5th edn (Univ. Oregon Press, 2007).
49. North TE et al. Prostaglandin E2 regulates vertebrate haematopoietic stem cell homeostasis. Nature 447, 1007–1011 (2007). [PubMed: 17581586]
50. Villefranc JA, Amigo J & Lawson ND Gateway compatible vectors for analysis of gene function in the zebrafish. Dev. Dyn 10.1002/dvdy.21354 (2007).
51. Lin HF et al. Analysis of thrombocyte development in CD41–GFP transgenic zebrafish. Blood 106, 3803–3810 (2005). [PubMed: 16099879]
52. Parsons MJ et al. Notch-responsive cells initiate the secondary transition in larval zebrafish pancreas. Mech. Dev 126, 898–912 (2009). [PubMed: 19595765]
53. Bussmann J, Wolfe SA & Siekmann AF Arterial-venous network formation during brain vascularization involves hemodynamic regulation of chemokine signaling. Development 138, 1717–1726 (2011). [PubMed: 21429983]
54. Scheer N & Campos-Ortega JA Use of the Gal4-UAS technique for targeted gene expression in the zebrafish. Mech. Dev 80, 153–158 (1999). [PubMed: 10072782]
55. Lawson ND & Weinstein BM In vivo imaging of embryonic vascular development using transgenic zebrafish. Dev. Biol 248, 307–318 (2002). [PubMed: 12167406]
56. Andrews S FastQC: a quality control tool for high throughput sequence data. https://www.bioinformatics.babraham.ac.uk/projects/fastqc/ (2010).
57. Bolger AM, Lohse M & Usadel B Trimmomatic: a flexible trimmer for Illumina sequence data. Bioinformatics 30, 2114–2120 (2014). [PubMed: 24695404]
58. Wang L, Wang S & Li W RSeQC: quality control of RNA-seq experiments. Bioinformatics 10.1093/bioinformatics/bts356 (2012).
59. Li H & Durbin R Fast and accurate long-read alignment with Burrows–Wheeler transform. Bioinformatics 10.1093/bioinformatics/btp698 (2010).
60. Trapnell C et al. Differential gene and transcript expression analysis of RNA-seq experiments with TopHat and Cufflinks. Nat. Protoc 7, 562–578 (2012). [PubMed: 22383036]
61. Wang L, Feng Z, Wang X, Wang X & Zhang X DEGseq: an R package for identifying differentially expressed genes from RNA-seq data. Bioinformatics 10.1093/bioinformatics/btp612 (2010).
62. Lee Y et al. FGF signalling specifies haematopoietic stem cells through its regulation of somitic Notch signalling. Nat. Commun 5, 5583 (2014). [PubMed: 25428693]
63. Kim AD et al. Discrete Notch signaling requirements in the specification of hematopoietic stem cells. EMBO J. 10.15252/embj.201488784 (2014).
64. Robu ME et al. p53 Activation by knockdown technologies. PLoS Genet. 3, 787–801 (2007).

65. Buenrostro JD, Wu B, Chang HY & Greenleaf WJ ATAC-seq: a method for assaying chromatin accessibility genome-wide. Curr. Protoc. Mol. Biol 2015, 21.29.1–21.29.9 (2015).

66. Wu J, Anczukow O, Krainer AR, Zhang MQ & Zhang C OLego: fast and sensitive mapping of spliced mRNA-seq reads using small seeds. Nucleic Acids Res. 41, 5149–5163 (2013). [PubMed: 23571760]

67. Heinz S et al. Simple combinations of lineage-determining transcription factors prime *cis*-regulatory elements required for macrophage and B cell identities. Mol. Cell 38, 576–589 (2010). [PubMed: 20513432]

68. Thorvaldsdóttir H, Robinson JT & Mesirov JP Integrative Genomics Viewer (IGV): high-performance genomics data visualization and exploration. Brief. Bioinform 14, 178–192 (2013). [PubMed: 22517427]

69. Dobin A et al. STAR: ultrafast universal RNA-seq aligner. Bioinformatics 29, 15–21 (2013). [PubMed: 23104886]

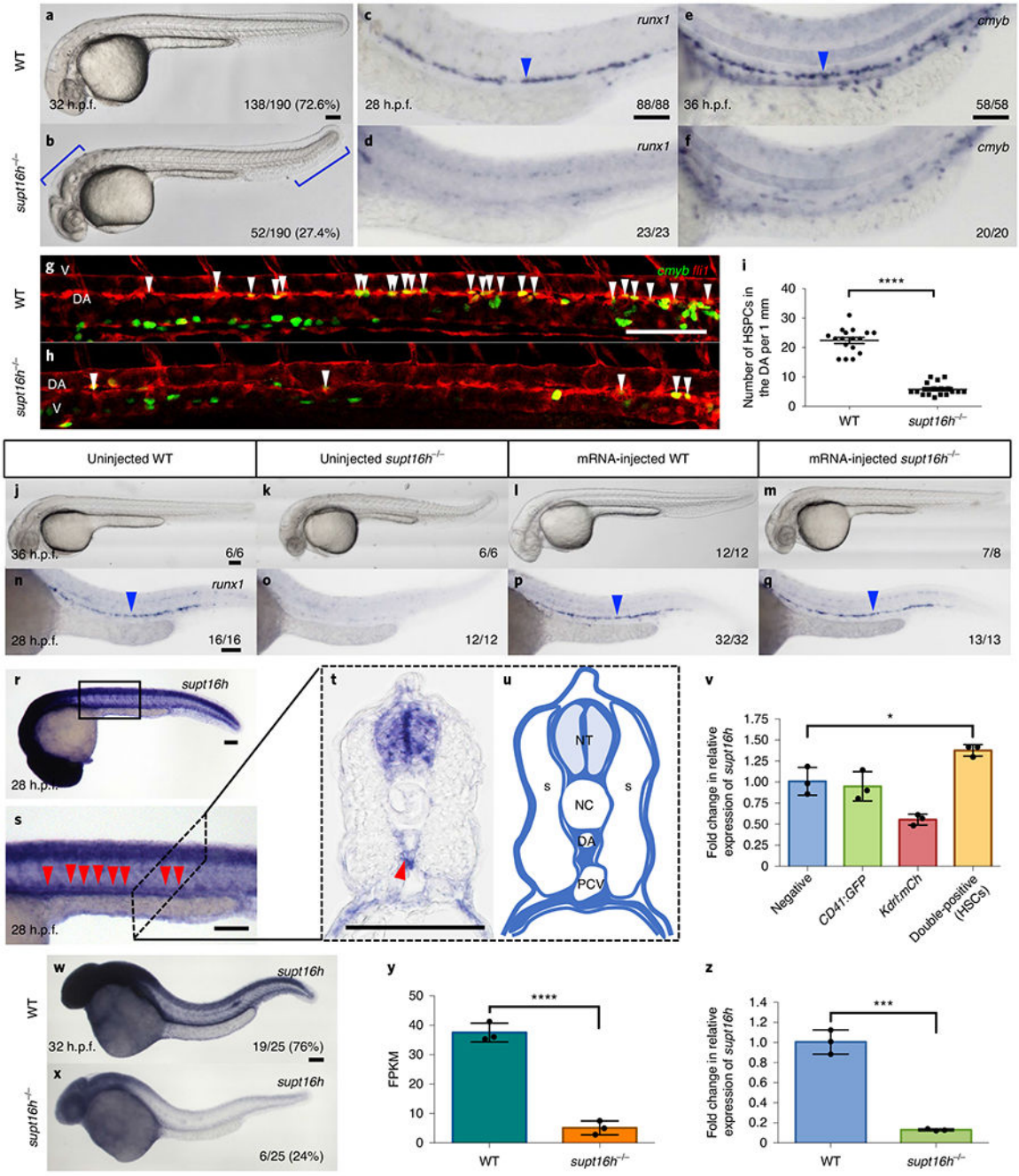


**Fig. 1 |. A forward genetic screen identifies *supt16h*$^{-/-}$ mutants that specifically lack HSPCs.**

**a,b**, Images of WT (**a**) and *supt16h*$^{-/-}$ (**b**) siblings at 32 h.p.f. The blue brackets highlight the morphological defects of the heads and tails of the mutants. **c-f**, WISH of the HSPC markers *runx1* at 28 h.p.f. (**c,d**) and *cmyb* at 36 h.p.f. (**e,f**) of WT (**c,e**) and *supt16h*$^{-/-}$ (**d,f**) siblings. **g,h**, Representative confocal images of WT (**g**) and *supt16h*$^{-/-}$ (**h**) siblings crossed with Tg(*cmyb:GFP; fli1:DsRed*) embryos. Double-positive HSPCs (yellow fluorescence) at 48 h.p.f. are indicated by white arrowheads. DA, dorsal aorta; V, vein. **i**, Number of double-positive HSPCs from **g,h**. Data are represented as the mean ± s.e.m.; $n = 17$. Two-tailed

Student's *t*-test, ****$P < 0.0001$. **j-q**, Injection of WT *supt16h* mRNA in WT and *supt16h*$^{-/-}$ sibling embryos. Bright-field images at 36 h.p.f. show morphological rescue of injected *supt16h*$^{-/-}$ embryos (**j-m**) and WISH of *runx1* at 28 h.p.f. (**n-q**). **r-u**, WISH of *supt16h* at 28 h.p.f. (**r**), with a magnified view of the boxed region in **r** along the dorsal aorta (**s**), a cross-sectional view (**t**) and a representative cartoon of **t** with the regions of expression coloured (**u**). NT, neural tube; S, somites; NC, notochord; DA, dorsal aorta; and PCV, post cardinal vein. The red arrowheads indicate the DA; $n = 4$. **v**, RT-qPCR analysis of *supt16h* in FACS-purified cells-double-positive (HSPCs), single-positive and negative cells-from Tg(*CD41:GFP; kdrl:mCherry*) embryos at 48 h.p.f. Data are represented as the mean ± s.d.; $n = 3$. One-way analysis of variance (ANOVA) with Tukey's post-hoc test, *$P = 0.0331$. **w,x**, WISH of *supt16h* on WT (**w**) and *supt16h*$^{-/-}$ (**x**) sibling embryos at 32 h.p.f. The percentages correlate with Mendelian segregation. **y,z**, Expression of *supt16h* in WT and *supt16h*$^{-/-}$ (pooled) sibling embryos at 32 h.p.f. determined through RNA-seq (**y**) and RT-qPCR (**z**). Data are represented as the mean ± s.d.; $n = 3$. Two-tailed Student's *t*-test, ****$P = 0.0001$ (**y**) and ***$P = 0.0002$ (**z**). FPKM, fragments per kilobase of transcript per million mapped reads. For RT-qPCR, the expression values are relative to those of the WT siblings. The blue arrowheads indicate HSPCs. Scale bars, 100 μm. For **a,b,w,x** the fractions represent the number of genotypic embryos over the clutch total. For **c-f**, **j-q** the fractions are the representative outcome for each genotyped group. Source data are provided.

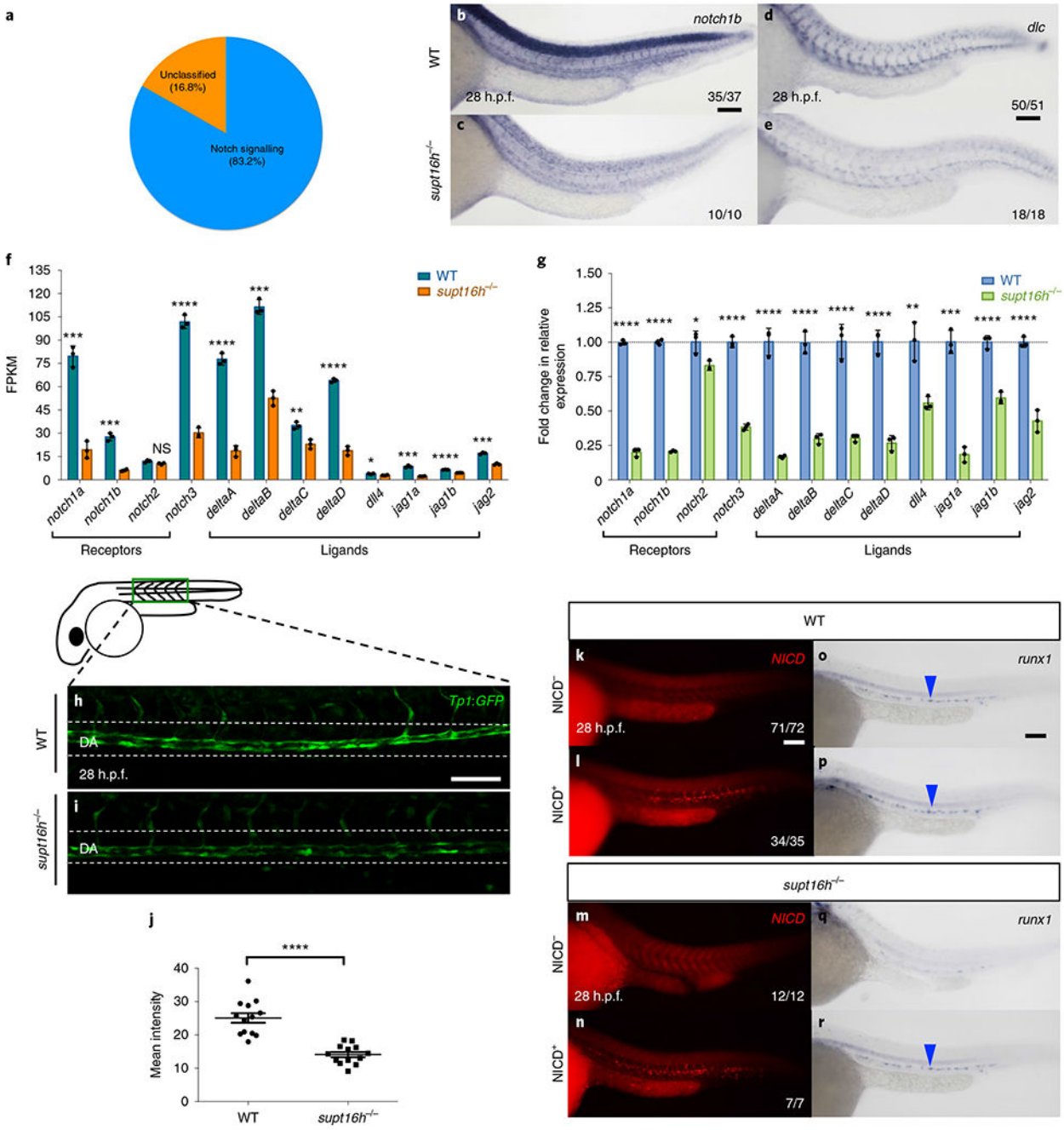


**Fig. 2 |. The Notch pathway is downregulated in *supt16h*$^{-/-}$ mutants.**

**a**, Pie chart of the downregulated pathways in *supt16h*$^{-/-}$ mutants based on Gene Ontology analysis ($\log_2$[fold change] > −1) of RNA-seq data. Fisher's exact test with Bonferroni correction, $P = 0.0334$. **b-e**, WISH of *notch1b* (**b,c**) and *dlc* (**d,e**) in WT (**b,d**) and *supt16h*$^{-/-}$ (**c,e**) sibling embryos. **f**, Expression levels of Notch genes based on RNA-seq. **g**, Expression levels, determined using RT-qPCR, of Notch genes in pooled embryos at 32 h.p.f. where expression is relative to the WT siblings (horizontal dotted line). FPKM, fragments per kilobase of transcript per million mapped reads. **f,g**, Data are represented as

the mean ± s.d.; $n = 3$. Two-tailed Student's $t$-test with Holm-Sidak correction for multiple comparisons; ****$P < 0.0001$, ***$P < 0.001$, **$P < 0.01$, *$P < 0.05$ and NS, not significant. **h,i**, Representative confocal images along the dorsal aorta (DA) of *supt16h*$^{-/-}$ (**i**) and WT (**h**) sibling embryos on a Tg(*Tp1 :GFP*) background at 28 h.p.f. **j**, Mean fluorescence intensity of *Tp1:GFP* along the DA from **h,i** calculated using ImageJ. Data are represented as the mean ± s.e.m.; $n = 13$. Two-tailed Student's $t$-test; ****$P < 0.0001$. **k-r**, Vascular-specific expression of NICD$^{+}$ (**l,n,p,r**) and NICD$^{-}$ (**k,m,o,q**) WT (**k,l,o,p**) and *supt16h*$^{-/-}$ (**m,n,q,r**; *supt16h*$^{+/-}$; cdh5:*gal4ff*×*supt16h*$^{+/-}$; *UAS-myc:NICD)* sibling embryos analysed at 28 h.p.f. by NICD immunohistochemistry (**k-n**) and *runx1* WISH (**o-r**). Representative images from two independent experiments. The blue arrowheads indicate HSPCs. For **b-e**, **k-r** the fractions are the representative outcome for each genotyped group. Scale bars, 100 μm. Source data are provided.

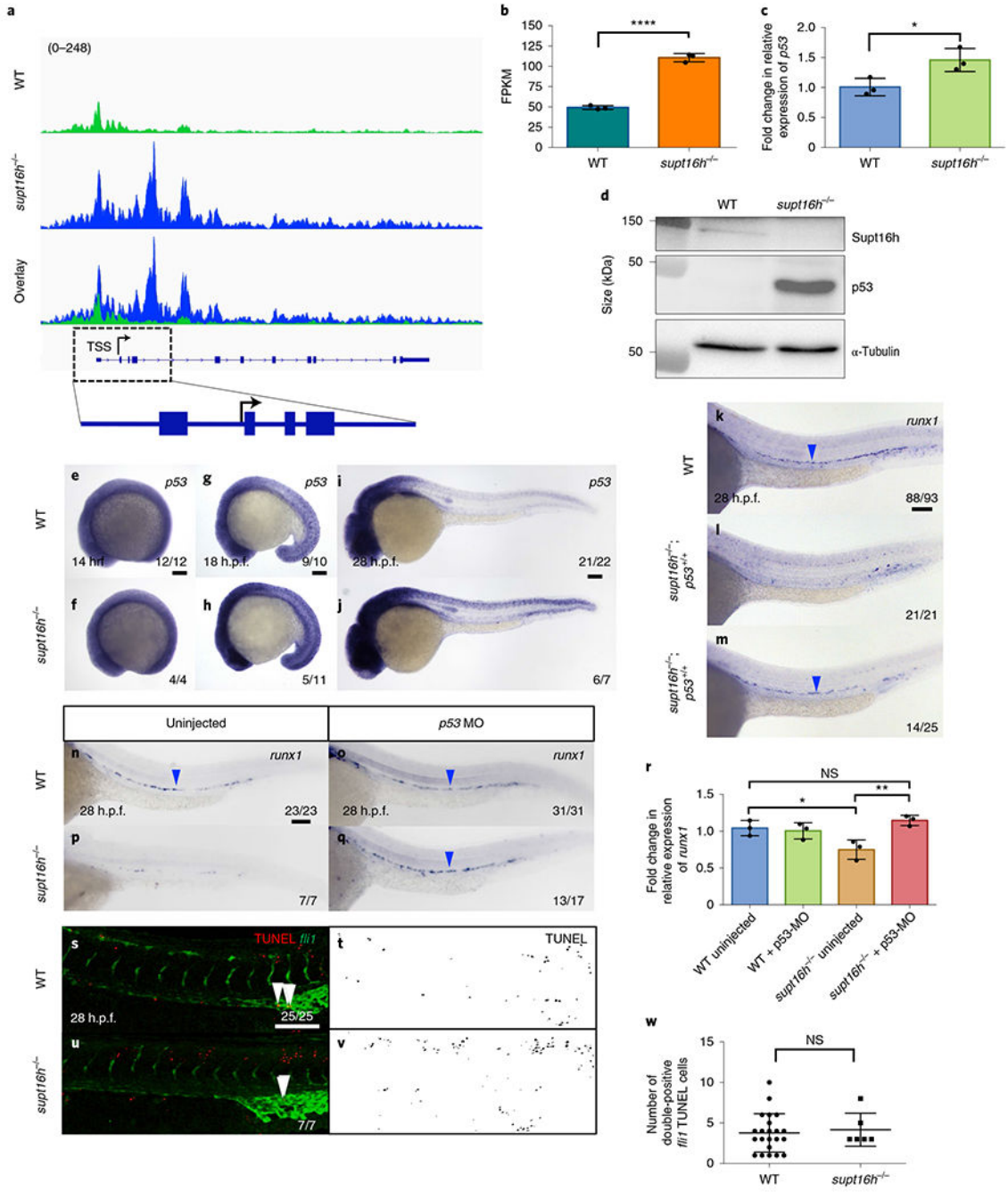


**Fig. 3 |. Induction of p53 in *supt16h*$^{-/-}$ mutants perturbs HSPC formation.**

**a**, Peaks of WT and *supt16h*$^{-/-}$ sibling embryos for *p53* ATAC-seq. The transcriptional start site (TSS), introns (blue lines) and exons (blue boxes) are shown (bottom). Value in parenthesis represents track height in pixels. **b,c**, Expression levels of *p53* in *supt16h*$^{-/-}$ and WT sibling embryos at 32 h.p.f. based on RNA-seq (**b**) and RT-qPCR (**c**). Data are represented as the mean ± s.d.; $n = 3$. Two-tailed Student's *t*-test, ****$P<0.0001$ (**b**) and *$P = 0.0317$ (**c**). **d**, Supt16h, p53 and α-tubulin western blots of *supt16h*$^{-/-}$ and WT sibling embryos at 32 h.p.f. Representative images from three biological replicates. Raw

unprocessed blots are available in the source data. **e-j**, WISH for *p53* expression in WT and *supt16h*$^{-/-}$ sibling embryos at 14 (**e,f**), 18 (**g,h**) and 28 h.p.f. (**i,j**). **k-m**, WISH for *runx1* of WT (**k**), *supt16h*$^{-/-}$*;p53*$^{+/+}$ (**l**) and *supt16h*$^{-/-}$*;p53*$^{-/-}$ (**m**) sibling embryos at 28 h.p.f. Representative of four biological replicates. **n-q**, WISH for *runx1* of WT (**n,o**) and *supt16h*$^{-/-}$ (**p,q**) sibling embryos injected with *p53*-MO (**o,q**) as well as uninjected controls (**n,p**). **r**, Expression levels of *runx1*, determined using RT-qPCR, in pooled embryos from **n-q** at 28 h.p.f. Data are represented as the mean ± s.d.; $n = 3$. One-way ANOVA with Tukey's post-hoc test; $^{*}P = 0.039$, $^{**}P = 0.0078$ and NS, not significant. **s-v**, TUNEL analysis of WT and *supt16h*$^{-/-}$ siblings crossed with *Tg(fli1i:GFP)* at 28 h.p.f. Confocal images of TUNEL, *fli1* and double-positive TUNEL+*fli1*$^{+}$ (yellow; indicated by white arrowheads; left), and TUNEL-only cells are shown (right). **w**, Number of double-positive TUNEL$^{+}$*fli1*$^{+}$ cells at 28 h.p.f. from **s-v**. Data are represented as the mean ± s.e.m.; $n = 22$ (WT) and 6 (*supt16h*$^{-/-}$). Two-tailed Student's *t*-test; NS, not significant. For the RT-qPCR, the expression values are relative to those of the WT siblings. The blue arrowheads indicate HSPCs. For **e-q**, **s** and **u** the fractions are the representative outcome for each genotyped group. Scale bars, 100 μm. Source data are provided.

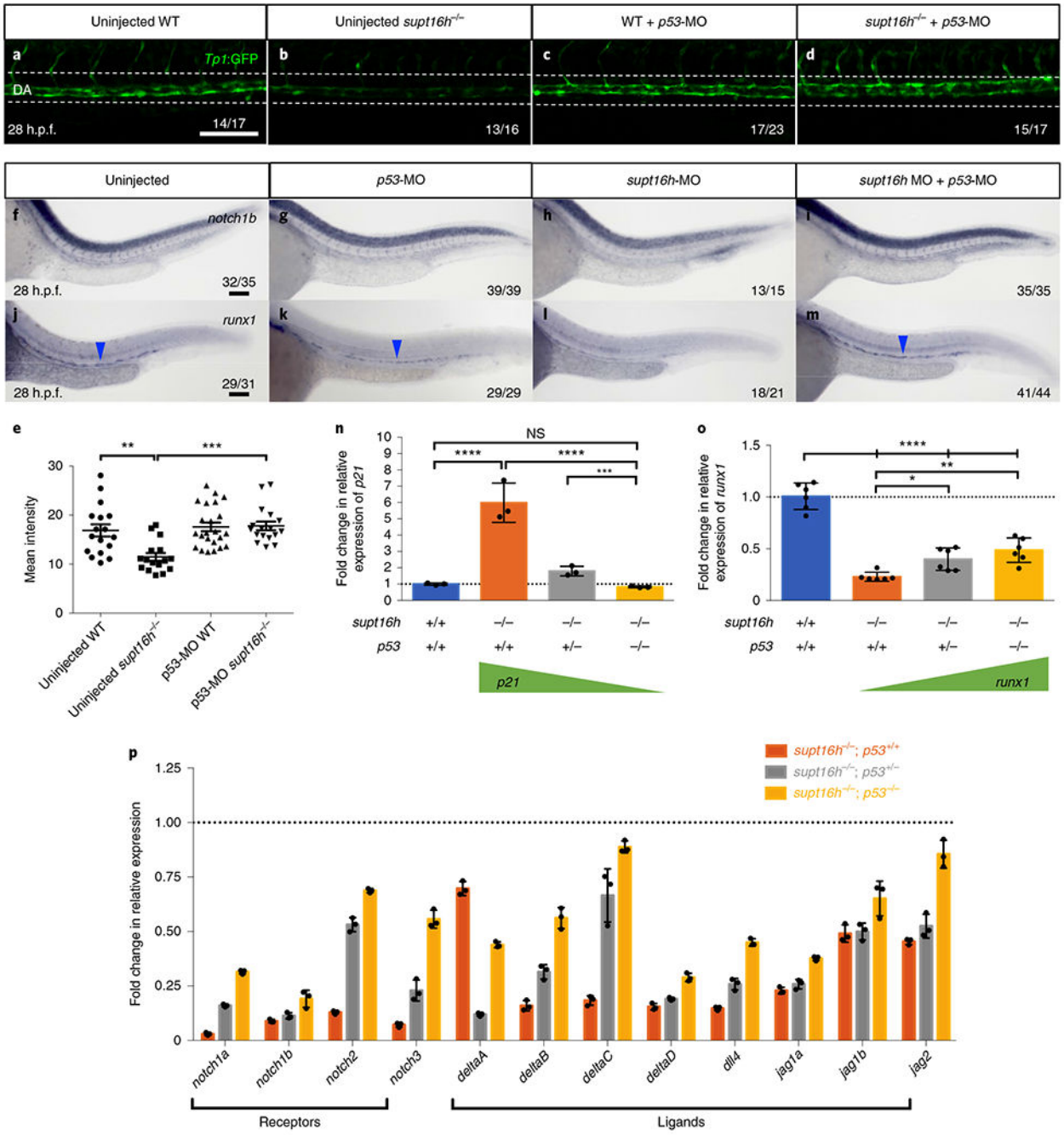


**Fig. 4 |. The transcription levels of the Notch genes are influenced by *p53* abundance.**

**a-d**, Representative confocal images of the dorsal aorta (DA) of *supt16h*$^{-/-}$ and WT sibling embryos on a Tg*(Tp1:GFP)* background injected with *p53*-MO (**c,d**) at 28 h.p.f. as well as uninjected controls (**a,b**). The white dotted lines represent the location of DA; *n*> 16. Scale bar, 25 μm. **e**, Mean fluorescence intensity of *Tp1:GFP* of the DA from **a-d** calculated in ImageJ based on Integrated Density. Data are represented as the mean ± s.e.m.; *n* = 17 (uninjected WT and p53-MO *supt16h*$^{-/-}$), 16 (uninjected *supt16h*$^{-/-}$) and 23 (p53-MO WT). One-way ANOVA with Tukey's post-hoc test, ***P* = 0.0021 and ****P* = 0.0002. **f-m**, WISH

for *notch1b* (**f-i**) and *runx1* (**j-m**) at 28 h.p.f. of uninjected embryos (**f,j**) and embryos injected with *p53*-MO (**g,k**), *supt16h*-MO (**h,l**) and *supt16h*-MO + *p53*-MO (**i,m**). The blue arrowheads indicate HSPCs. **n,o**, Expression levels at 32 h.p.f. of *p21* (**n**) and *runx1* (**o**), determined by RT-qPCR, in WT and *supt16h*$^{-/-}$ sibling embryos that are *p53*$^{+/+}$*p53*$^{+/-}$ or *p53*$^{-/-}$. Data are represented as the mean ± s.d.; $n = 3$ (**n**) and 6 (**o**). One-way ANOVA with Tukey's post-hoc test; ****$P < 0.0001$, ***$P = 0.0002$, **$P = 0.0021$, *$P = 0.0492$ and NS, not significant. **p**, Expression levels at 32 h.p.f., determined by RT-qPCR (3′ ends), of Notch receptors and ligands in *supt16h*$^{-/-}$ embryos that are *p53*$^{+/+}$, *p53*$^{+/-}$ or *p53*$^{-/-}$. Data are represented as the mean ± s.d.; $n = 3$). **n-p**, The expression values are relative to those of the WT siblings (horizontal dotted line). Scale bar, 100 μm. Source data are provided.

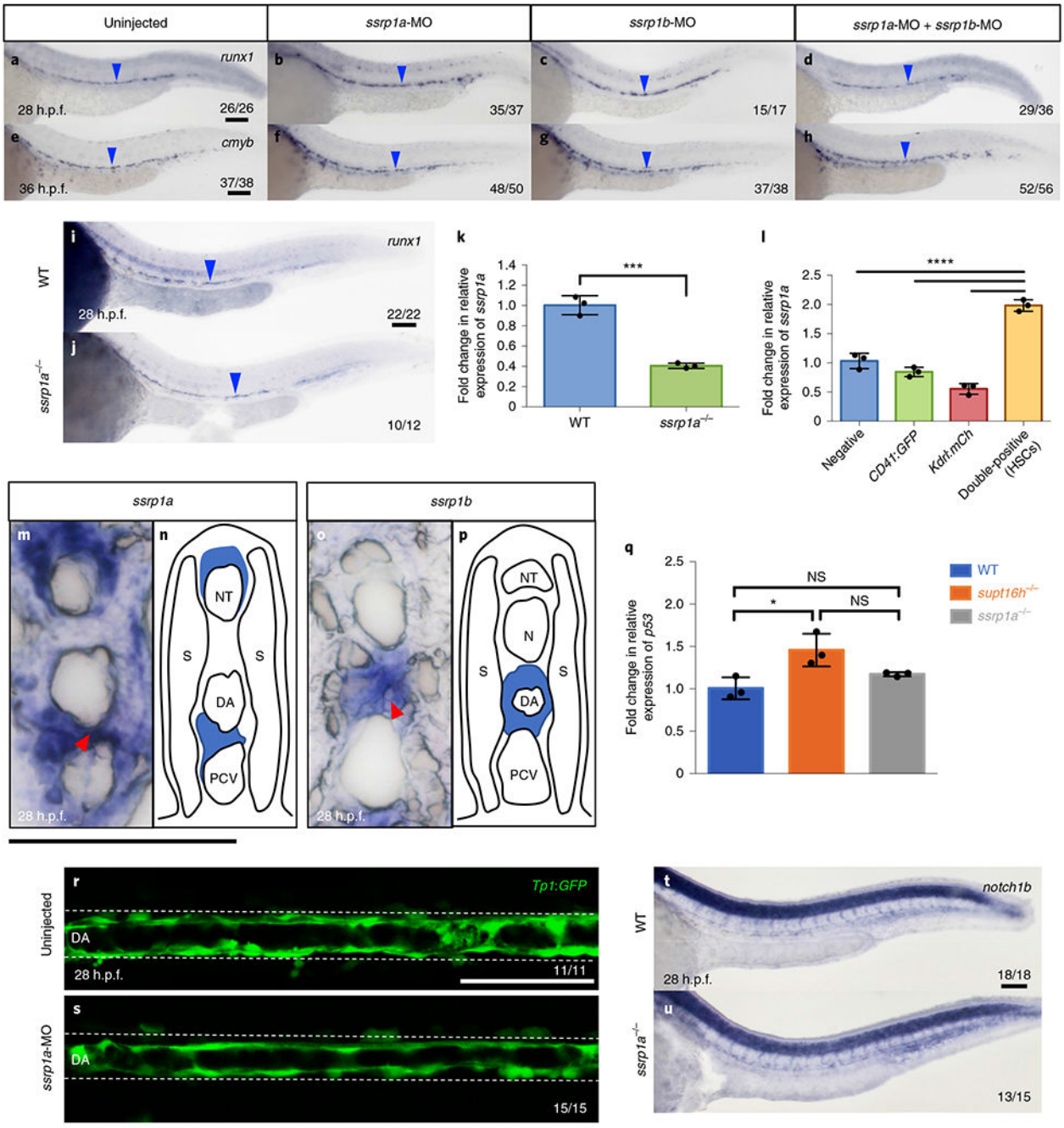


**Fig. 5 |. HSPC specification is unaffected by *ssrp1*.**

**a-h**, WISH for *runx1* (**a-d**) and *cmyb* (**e-h**) at 28 and 36 h.p.f., respectively, of embryos injected with *ssrp1a*-MO, *ssrp1b*-MO or both. **i,j**, WISH for *runx1* of WT (**i**) and *ssrp1a*$^{-/-}$ (**j**) sibling embryos at 28 h.p.f. **a-j**, The blue arrowheads indicate HSPCs. **k**, Expression of *ssrp1a* in WT and *ssrp1a*$^{-/-}$ sibling embryos at 32 h.p.f. based RT-qPCR. Data are represented as the mean ± s.d.; $n = 3$. Two-tailed Student's *t*-test, ***$P = 0.0004$. **l**, Expression of *ssrp1a* in FACS-purified cells (double-positive (HSPCs), single-positive and negative cells) from Tg(*CD41:GFP;kdrl:mCherry)* embryos at 48 h.p.f. determined by RT-

qPCR. Data are represented as the mean ± s.d.; $n = 3$. One-way ANOVA with Tukey's post-hoc test; ****$P < 0.0001$, **$P = 0.0019$ and *$P = 0.0328$. **m-p**, Cross section of *ssrp1a* (**m,n**) and *ssrp1b* (**o,p**) WISH at 28 h.p.f. The red arrowheads indicate expression at the floor of the dorsal aorta. **n,p**, Representative cartoons showing expression from **m** and **o**, respectively. NT, neural tube; S, somites; DA, dorsal aorta; and PCV, post cardinal vein. **q**, Expression of *p53* in WT, *supf16h*$^{-/-}$ and *ssrp1a*$^{-/-}$ embryos at 32 h.p.f. determined by RT-qPCR. Data are represented as the mean ± s.d.; $n = 3$. One-way ANOVA with Tukey's post-hoc test; *$P = 0.0147$; and NS, not significant. **r,s**, Representative confocal images along the dorsal aorta (DA) of Tg(*Tp1:GFP*) embryos injected with *ssrp1a*-MO (**s**), as well as uninjected controls (**r**), at 28 h.p.f. based on one independent experiment. **t,u**, WISH for *nofch1b* expression in WT (**t**) and *ssrp1a*$^{-/-}$ sibling (**u**) embryos at 28 h.p.f. **k,l,q**, The expression values are relative to those of the WT siblings. For **a-j**, **r-u** the fractions are the representative outcome for each genotyped group. Scale bars, 100 μm. Source data are provided.

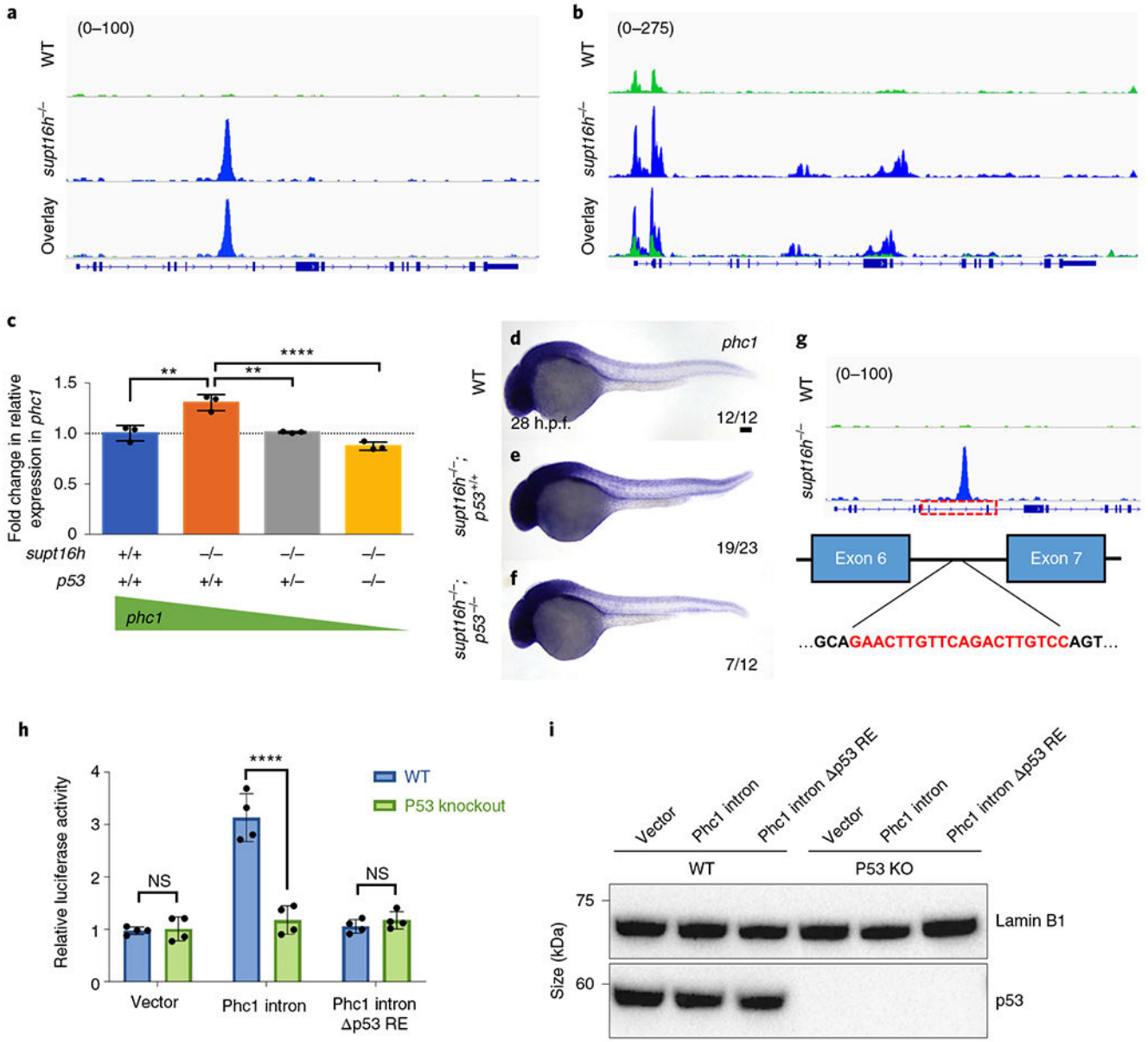


**Fig. 6 |. p53 augments *phc1* expression in *supt16h* mutants.**

**a**, Image of *phc1* peaks in WT (top) and *supt16h*$^{-/-}$ (middle) siblings based on p53 ChIP-seq, with the location of the introns (blue lines) and exons (blue boxes) indicated (bottom). **b**, ATAC-seq peaks for *phc1* in WT and *supt16h*$^{-/-}$ sibling embryos. **c**, Expression of *phc1*, determined by RT-qPCR, at 32 h.p.f. in WT and *supt16h*$^{-/-}$ sibling embryos that are *p53*$^{+/+}$, *p53*$^{+/-}$ or *p53*$^{-/-}$. The expression values are relative to those of the WT siblings (horizontal dotted line). Data are represented as the mean ± s.d.; $n = 3$. One-way ANOVA with Tukey's post-hoc test, **** $P$ 0.0001 and ** $P = 0.001$. **d-f**, WISH analysis of *phc1* in WT (d), *supt16h*$^{-/-}$;*p53*$^{+/+}$ **(e)** and *supt16h*$^{-/-}$;*p53*$^{-/-}$ **(f)** sibling embryos at 28 h.p.f. Scale bar, 100 μm. **g**, Predicted p53 responsive element in the *phc1* allele of *Danio rerio.* The schematic has been overlaid with p53 ChIP-seq peaks of *phc1*. **h**, Relative luciferase activity of a HCT116

p53-knockout (Δp53 RE) cell line to assess the p53-dependent transactivation of the predicted responsive element in *phc1*. Data are represented as the mean ± s.d.; $n = 4$. Two-way ANOVA with Holm-Sidak correction for multiple comparisons; **** $P < 0.00001$ and NS, not significant. **i**, Western blot of the whole-cell lysates of Δp53 RE and WT HCT116 cell lines probed for p53. Raw unprocessed blots and quantification data are available. For **a-c** value in parenthesis represents track height in pixels.

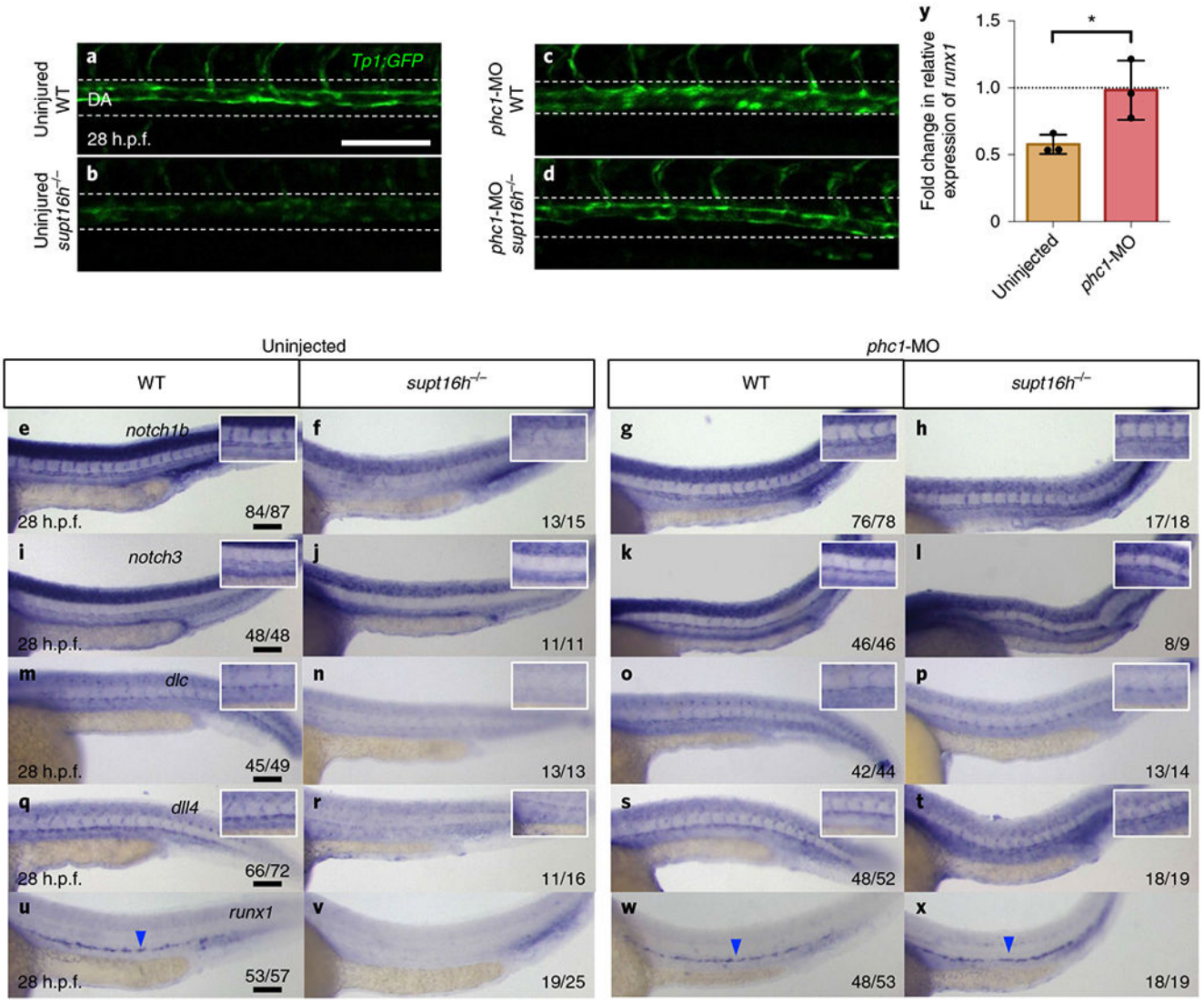


**Fig. 7 |. Expression of *phc1* influences Notch-gene transcription and HSPC specification.**

**a-d**, Representative confocal images, at 28 h.p.f., along the dorsal aorta (DA) of Tg(*Tp1:GFP*) embryos on WT (**a,c**) and *supt16h*$^{-/-}$ (**b,d**) sibling backgrounds injected with *phc1*-MO (**c,d**) as well as uninjected controls (**a,b**). $n = 15$ (WT), 5 (*supt16h*$^{-/-}$), 16 (WT +*phc1*-MO) and 4 (*supt16h*$^{-/-}$ + *phc1*-MO). **e-x**, WISH of WT and *supt16h*$^{-/-}$ sibling uninjected controls (**e,f,i,j,m,n,q,r,u,v**) and embryos injected with *phc1*-MO (**g,h,k,l,o,p,s,t,w,x**) probed for *notch1b* (**e-h**), *notch3* (**i-l**), *dlc* (**m-p**), *dll4* (**q-t**) and *runx1* (**u-x**) at 28 h.p.f. Insets: magnified views of the dorsal aorta and intersomitic vessels. The blue arrowheads indicate HSPCs. **y**, Expression of *runx1*, determined by RT-qPCR, of *supt16h*$^{-/-}$ embryos injected with *phc1*-MO at 28 h.p.f. Data are represented as the mean ± s.d.; $n = 3$. Two-tailed Student's *t*-test, $P = 0.0393$. The expression values are relative to those of the WT siblings (horizontal dotted line). For **e-x** the fractions are the representative outcome for each genotyped group. Scale bars, 100 μm. Source data provided.